SIAM J. Applied Dynamical Systems
Vol. 19, No. 1, pp. 366–411

Bifurcations on Fully Inhomogeneous Networks*

Punit Gandhi†, Martin Golubitsky‡, Claire Postlethwaite§, Ian Stewart¶, and Yangyang Wang‖

Abstract. Center manifold reduction is a standard technique in bifurcation theory, reducing the essential features of local bifurcations to equations in a small number of variables corresponding to critical eigenvalues. This method can be applied to admissible differential equations for a network, but it bears no obvious relation to the network structure. A fully inhomogeneous network is one in which all nodes and couplings can be different. For this class of networks, there are general circumstances in which the center manifold reduced equations inherit a network structure of their own. This structure arises by decomposing the network into path components, which connect to each other in a feedforward manner. Critical eigenvalues can then be associated with specific components, and the network structure on the center manifold depends on how these critical components connect within the network. This observation is used to analyze codimension-1 and codimension-2 local bifurcations. For codimension-1, only one critical component is involved, and generic local bifurcations are saddle-node and standard Hopf. For codimension-2, we focus on the case when one component is downstream from the other in the feedforward structure. This gives rise to four cases: steady or Hopf upstream combined with steady or Hopf downstream. Here the generic bifurcations, within the realm of network-admissible equations, differ significantly from generic codimension-2 bifurcations in a general dynamical system. In each case, we derive singularity-theoretic normal forms and unfoldings, present bifurcation diagrams, and tabulate the bifurcating states and their stabilities.

Key words. networks, bifurcation theory, normal forms, codimension, Hopf bifurcation, mode interactions

AMS subject classifications. 34F10, 37G05, 37G15

DOI. 10.1137/18M1230736

1. Introduction.

The structure and behavior of networks is a rapidly developing area with applications to many branches of science (Stewart (2004); Newman, Barabási, and Watts

*Received by the editors December 5, 2018; accepted for publication (in revised form) September 17, 2019; published electronically February 4, 2020.
https://doi.org/10.1137/18M1230736
Funding: This research was supported in part by National Science Foundation grant DMS-1440386 to the Mathematical Biosciences Institute. The second and fourth authors thank the Department of Mathematics of the University of Auckland for its support and hospitality. The research of the third author was supported by the Marsden Fund Council from New Zealand Government funding, managed by Royal Society Te Aparangi. The third author also acknowledges the generous hospitality of the Mathematical Biosciences Institute.
†Mathematical Biosciences Institute, Ohio State University, Columbus, OH 43215. Current address: Department of Mathematics & Applied Mathematics, Virginia Commonwealth University, Richmond, VA 23284-2014 (gandhipr@vcu.edu).
‡Department of Mathematics, Ohio State University, Columbus, OH 43215 (golubitsky.4@osu.edu).
§Department of Mathematics, University of Auckland, Auckland, 1142, New Zealand (c.postlethwaite@auckland.ac.nz).
¶Mathematics Institute, University of Warwick, Coventry, CV4 7AL, UK (i.n.stewart@warwick.ac.uk).
‖Mathematical Biosciences Institute, Ohio State University, Columbus, OH, 43215. Current address: Department of Mathematics, University of Iowa, Iowa City, IA 52242-1419 (yangyang-wang@uiowa.edu).

(2006); Lu et al. (2016)). The research literature now extends to many thousands of papers. The mathematical methods employed include graph theory, algebra, probability, combinatorics, topology, and extensive computer simulations.

A topic of considerable interest is the study of dynamics and bifurcations for networks of coupled dynamical systems (Stewart, Golubitsky, and Pivato (2003); Golubitsky, Stewart, and Török (2005); Golubitsky and Stewart (2006)). In this context, a network is a directed graph whose edges are classified into distinct types, one for each type of coupling. In many examples, the network structure influences the dynamics that can be expected to occur generically, leading to behavior that does not arise generically in a general dynamical system. Therefore the methodology of modern nonlinear dynamics (Guckenheimer and Holmes (1983)), although widely applicable, often has to be adapted to the network context before it can be used.

Each network architecture determines a class of *admissible maps* and associated *admissible differential equations (ODEs)*, which respect the structure of the network. The dynamics of each node is determined by the node itself and all nodes from which it receives inputs. The type of coupling involved in the inputs is also taken into account. In particular, issues such as symmetry and synchrony can be studied systematically using this formalism.

One of the powerful methods of bifurcation theory is center manifold reduction (Carr (1981)). This makes it possible to analyze steady-state and Hopf bifurcations analytically, using coordinate changes to determine local polynomial approximations that capture the bifurcation behavior. In general, these coordinate changes are not well adapted to the network structure of coupled systems. In fact, at first sight there seems to be little connection between the network structure of a dynamical system and the structure of a center manifold reduction. We show that in certain specific circumstances such a connection exists, and it sometimes leads to unexpected bifurcations and dynamics. We examine this phenomenon in detail, with rigorous proofs based on singularity-theoretic normal forms; see, for example, Martinet (1982); Golubitsky and Schaeffer (1985).

A similar observation has been made for a very different class of networks. Rink and Sanders (2014, 2015); Nijholt, Rink, and Sanders (2016, 2017); Nijholt (2018) have developed an elegant approach to synchrony in networks, and technical issues concerning center manifold reduction, based on graph fibrations (see Boldi and Vigna (2002); Deville and Lerman (2015)). In particular, their results show that in some cases a center manifold reduction of a network system has a network structure of its own, inherited from the original network. Their viewpoint is algebraic, and it is most effective for a special class of homogeneous networks: networks where every node receives exactly one input of each of a specific list of types. Moreover, their strongest results apply to feedforward networks, in which there are no closed directed cycles. Soares (2018) also considers bifurcations in feedforward quotient networks and their effect on bifurcations in the original network.

Here we consider a class of networks that is almost the exact opposite of this special class: *fully inhomogeneous* networks, in which all nodes and arrows have distinct types (Golubitsky and Stewart (2017)). The graph structure of such networks carries with it dynamical notions, notably admissible maps and systems of ODEs. For a fully inhomogeneous n-node network, the admissible ODEs are determined by the connections, and take the form

$$\dot{x}_j = f_j(x_j, x_{\sigma_j(1)}, \dots, x_{\sigma_j(s_j)}), \qquad j = 1, \dots, n, \tag{1.1}$$

where $\sigma_j(1), \ldots, \sigma_j(s_j)$ enumerate the s_j nodes that connect to node j. Because all edges of the network have different types, the function f_j is arbitrary, subject to having the appropriate domain and range, and the x_j are elements of finite-dimensional real vector spaces.

Biochemical networks (Best, Nijhout, and Reed (2010)), gene regulatory networks (Borisuk and Tyson (1998)), and food webs (Fussman and Heber (2002); Allesin and Pascual (2008)) are examples of such systems. Therefore the dynamics and bifurcations for this class of networks deserve attention. Here we consider the two standard types of local bifurcations, steady-state and Hopf, on any dynamical system that is admissible for a fully inhomogeneous network. We also consider mode interactions, where two local bifurcations occur simultaneously at the same parameter values. We show that in mode interactions the center manifold determined by the critical eigenvalues inherits its own network structure.

These observations make it possible to apply an appropriate version of singularity theory, adapted to the network of the center manifold and the type of local bifurcation. This allows us to determine a normal form for the bifurcation and to compute its universal unfolding—a parametrized family of perturbations that captures the structure of all such families in a sense explained in section SM2 of the supplementary materials for this manuscript, linked from the main article webpage.

We do not include a distinguished bifurcation parameter as in Golubitsky and Schaeffer (1985), which would complicate the calculations considerably. Instead, the bifurcation parameters are included as universal unfolding parameters. It is also convenient to work with the special case in which all nodes have a one-dimensional phase space, which we take to be the real line $\mathbb{R}$. However, Appendix A shows that a network with multidimensional nodes can be reduced to one with one-dimensional nodes and the same admissible maps. Using this reduction, our results can be transferred directly to fully inhomogeneous networks for which node phase spaces have any finite dimension.

Organization of paper. The main principle underlying this paper is introduced in section 2. Local bifurcation in the dynamics of (1.1) occurs when the Jacobian has critical eigenvalues, which can be associated with specific path components. See Lemma 2.3. Center manifolds are in general not unique, but any choice captures the bifurcation structure. We show that with a suitable choice, the dynamics on the center manifold can be interpreted as a dynamical system for a simplified network. In section 2.3, we interpret our results specifically in terms of the sort of dynamics we expect to be observed in each of the nodes of the original network. Different behavior may be seen depending on whether the observed node is upstream or downstream of where the bifurcation(s) occur, as well as other couplings between nodes in the network. Several examples of results for specific networks are given in section 2.4.

The rest of the paper analyzes the most common local bifurcations, those of codimension-1 or codimension-2. The codimension is the minimal number of parameters for such a bifurcation to occur generically in a parametrized family (Guckenheimer and Holmes, 1983, p. 122). Proofs of these main results are presented in sections SM1–SM6 of the supplementary materials.

The generic codimension-1 steady-state and Hopf bifurcations are described in section 3, without proofs at this stage. Theorem 3.1 describes steady-state bifurcation, and Theorem 3.7 describes Hopf bifurcation. Abstractly these bifurcations are the same as those expected for

a network with general vector fields, that is, with *all-to-all* coupling of the variables. This result is plausible, but the proofs involve some subtleties because a path component need not be all-to-all connected. We therefore postpone proofs to section SM1. The impact of the bifurcations on the full network is also considered; unsurprisingly, only the nodes within or downstream from the critical path component feel this influence. Thus, there are two kinds of codimension-1 bifurcation for each path component in the network: one for steady-state bifurcation and one for Hopf bifurcation.

The structure of center manifolds for the codimension-2 mode interaction bifurcations that we consider is described in section 4. The main result is Theorem 4.3, which states that the dynamics on the center manifold is that of a two-node feedforward network.

The results of the bifurcation analyses on the center manifold are stated in section 5. The proofs are again postponed to SM3–SM6. The four mode interactions (steady-state/steady-state, Hopf/steady-state, steady-state/Hopf, and Hopf/Hopf) are discussed in successive subsections. In each subsection, we state the singularity-theoretic normal form for the mode interaction, compute its codimension, and obtain a universal unfolding. The equilibria and/or periodic states involved are tabulated, along with their stabilities, and bifurcation diagrams are presented.

Finally, Appendix A describes, in the context of fully inhomogeneous networks, a general construction that converts any network with higher-dimensional node phase spaces into an "expanded" network with one-dimensional node phase spaces, without changing the space of admissible maps. This construction justifies our running assumption that node phase spaces are one-dimensional and implies that the same results are valid for general node phase spaces.

2. Path components and feedforward structure.

Our strategy is to give a systematic and general description of the constraints on center manifold reduced equations that are associated with mode interactions in fully inhomogeneous networks. To that end, we enumerate a set of "critical components" and associated "central networks" that capture the possible bifurcations that can occur generically for any given inhomogeneous network. Throughout this paper, "path" refers to a directed path.

Definition 2.1. *Node q is* downstream *from node p if there exists a path from p to q. Node p is* upstream *from node q if q is downstream from p. Nodes p and q are* path equivalent*, denoted by $p \sim q$, if node p is both upstream and downstream from node q.*

Definition 2.2. *A* path component *is an equivalence class of nodes under path equivalence. Path component Q is* downstream *from path component P if there exist a node p in component P and a node q in component Q such that q is downstream from p. Path component P is* upstream *from component Q if Q is downstream from P.*

The notions of *downstream* and *upstream* are relational concepts that play a key role in determining the central network.

The path components are connected in a feedforward manner (the graph-theoretic term is "acyclic": no closed path). This is well known in the theory of directed graphs (Schröder (2002)). The directed graph induced on the components is called the *component graph* or *condensation* of the original network (Eppstein (2016)). The proof is simple. Write $i \preceq j$ if there is a path from node i to node j (including the trivial path from i to itself). Then $\preceq$ is

a preorder. The relation $i \sim j$ defined by $i \preceq j$ and $j \preceq i$ is an equivalence relation on nodes, and the path components are the equivalence classes. Now $\preceq$ induces a partial order on the set of path components.

Recall that every finite partially ordered set has a consistent total order. The proof is by induction on the number m of elements in the set. This is trivial for $m = 1$. For $m > 1$, choose a minimal element (nothing smaller in the partial order) and number it m. Remove the element called m and, by induction, number the remaining elements $1, \dots, m-1$.

The total order on path components determines a feedforward structure on the path components. It follows that we can order the nodes so that the Jacobian matrix of (1.1) is block lower triangular. To see this, let $X_j \in \mathbb{R}^{\alpha_j}$ be the coordinates in the jth path component C_j, where α_j is the number of nodes in C_j. The coordinates of an admissible vector field for a network with m path components have the form

$$\dot{X}_j = F_j(X_j, X_1, \dots, X_{j-1}), \qquad j = 1, \dots, m. \tag{2.1}$$

In general, the F_j are not arbitrary, since they arise from (1.1) by collecting variables, nor are the F_j defined uniquely from the f_j. Lemma 2.3 then follows.

Lemma 2.3. *The Jacobian matrix J of (2.1) at any point is block lower triangular with the form*

$$J = \begin{bmatrix} J_1 & & & \\ * & J_2 & \mathbf{0} & \\ * & * & \ddots & \\ * & * & \cdots * & J_m \end{bmatrix}, \tag{2.2}$$

where J_j is the $\alpha_j \times \alpha_j$ Jacobian matrix of the jth path component.

The blocks in this decomposition are unique up to reordering nodes within each path component. The ordering of the blocks need not be unique, but it must be compatible with the feedforward partial order.

2.1. Critical components. By (1.1), translation preserves admissibility, so we may translate coordinates so that any given equilibrium of (2.1) is at the origin. The form of J in (2.2) implies that the eigenvalues of J are the union of the eigenvalues of $J_1, \dots, J_m$ (including multiplicities). Since the J_i are unique up to reordering of the component nodes, they are unique up to similarity. Therefore the critical eigenvalues are invariants.

Definition 2.4. *At an equilibrium, the path component C_j is* critical *if an eigenvalue of J_j is on the imaginary axis.*

For example, Lemma 2.3 implies that a codimension-2 Hopf/steady-state bifurcation can be associated with either one or two critical components. Moreover, when there are two critical components, we know which is Hopf and which is steady-state.

This paper classifies the behavior of all codimension-1 and certain codimension-2 local bifurcations on a given fully inhomogeneous network. Codimension-2 bifurcations can occur in two types: nonlinear degeneracies of a codimension-1 bifurcation or mode interactions occurring from the nonlinear interaction of two codimension-1 bifurcations. Moreover, in

networks, mode interactions can occur in several ways, related to how the critical components lie within the network. Specifically, mode interactions can occur with two critical eigenvalues

- in the same critical component,
- in two critical components where one is downstream of the other,
- in two critical components where neither component is downstream of the other.

In this paper, we consider in detail only the second possibility. We show that these codimension-2 bifurcations are qualitatively different from mode interactions in general systems of differential equations. The third possibility is easy to analyze: the two codimension-1 bifurcations are independent. We believe, but have not proved, that the first possibility behaves just like codimension-2 bifurcations in general systems.

2.2. The central network. For a given bifurcation from an equilibrium in a fully inhomogeneous network, we construct a central network and show that the dynamics on the center manifold (Carr (1981)) of the full network are diffeomorphic to the dynamics on the center manifold of the central network. See Theorem 2.10.

Definition 2.5. *Suppose that the network $\mathcal{G}$ has at least one critical path component. The* central network $\mathcal{C}$ *of $\mathcal{G}$ is defined by the following:*

(a) *The path components of $\mathcal{C}$ are the path components of $\mathcal{G}$ that are both upstream from some critical component and downstream from some critical component.*
(b) *The arrows in $\mathcal{C}$ are the arrows of $\mathcal{G}$ that connect nodes in $\mathcal{C}$.*

Remark 2.6. If $\mathcal{G}$ has only one critical path component, the central network $\mathcal{C}$ consists of the nodes in the critical component and the arrows that connect nodes in that critical component. This follows since nodes are both upstream and downstream from the same path component if and only if they lie in that path component.

Lemma 2.7. *The central network can be constructed as follows:*

(a) *Let $\mathcal{X}$ be the union of all path components that are not downstream from any critical path component.*
(b) *Let $\mathcal{Z}$ be the union of all path components in $\mathcal{G} \setminus \mathcal{X}$ that are not upstream from any critical component.*

Then the nodes in the central network $\mathcal{C}$ consist of nodes in $\mathcal{G}$ that are not in $\mathcal{X} \cup \mathcal{Z}$. The arrows are those whose head and tail are in $\mathcal{C}$. The nodes in $\mathcal{G}$ decompose as a disjoint union

$$\mathcal{G} = \mathcal{X} \dot\cup \mathcal{C} \dot\cup \mathcal{Z}. \tag{2.3}$$

Proof. By (a), $\mathcal{X} \cap \mathcal{C} = \emptyset$. By (b), $\mathcal{Z} \cap \mathcal{C} = \emptyset$. Hence the nodes in the central network are contained in the complement of nodes in $\mathcal{X} \cup \mathcal{Z}$. Conversely, nodes in the complement of $\mathcal{X}$ and $\mathcal{Z}$ are both upstream and downstream from some critical components, and hence in $\mathcal{C}$. Finally, (b) implies that $\mathcal{X} \cap \mathcal{Z} = \emptyset$, so (2.3) holds. ∎

Using the notation in Lemma 2.7 we have the following.

Lemma 2.8.

(a) *Tails of arrows in $\mathcal{G}$ whose heads are in $\mathcal{X}$ must also be in $\mathcal{X}$.*
(b) *Tails of arrows in $\mathcal{G}$ whose heads are in $\mathcal{C}$ must be in either $\mathcal{C}$ or $\mathcal{X}$.*
(c) *Tails of arrows in $\mathcal{G}$ whose heads are in $\mathcal{Z}$ can be in any node in $\mathcal{G}$.*

Label the nodes of $\mathcal{G}$ so that the first n_x are in $\mathcal{X}$, the last n_z are in $\mathcal{Z}$, and the remaining nodes are all in the central network $\mathcal{C}$. Then Lemma 2.8 implies that an admissible ODE for $\mathcal{G}$ has the form

$$\dot{X} = F(X), \tag{2.4a}$$

$$\dot{Y} = G(X, Y), \tag{2.4b}$$

$$\dot{Z} = H(X, Y, Z), \tag{2.4c}$$

where $X \in \mathbb{R}^{n_x}$, $Y \in \mathbb{R}^{n_y}$, and $Z \in \mathbb{R}^{n_z}$. Since all critical components are in the central network, the eigenvalues of the Jacobians $D_X F(0)$ and $D_Z H(0)$ all have nonzero real part.

Relabeling coordinates, we can assume that the bifurcation point of (2.4) is at $(0, 0, 0)$. Specifically, we assume $F(0) = 0$. Now (2.4) implies the following.

Theorem 2.9. *A center manifold of* (2.4) *is contained in the subspace* $X = 0$. *That is, the coordinates of nodes that are not downstream from any critical node are equal to* 0.

We will prove that the center manifold dynamics of the central network system

$$\dot{Y} = G(0, Y)$$

is conjugate to the center manifold dynamics of the vector field

$$\begin{aligned} \dot{X} &= 0, \\ \dot{Y} &= G(0, Y), \\ \dot{Z} &= H(0, Y, Z) \end{aligned} \tag{2.5}$$

on $\mathcal{G}$. Without loss of generality, we can drop the dependence of G, H on the zero coordinates, leading to

$$\dot{Y} = G(Y), \tag{2.6a}$$

$$\dot{Z} = H(Y, Z). \tag{2.6b}$$

Our goal is to prove that the dynamics on the center manifold of (2.6a) is conjugate to the dynamics of the center manifold of (2.6).

Denote the m-dimensional center subspace of (2.6) by $E^c_{y,z}$, and denote the m-dimensional center subspace of the central network with the vector field (2.6a) by E^c_y. Let $\pi_y : \mathbb{R}^{n_y} \times \mathbb{R}^{n_z} \to \mathbb{R}^{n_y}$ be projection, $\pi_y(Y, Z) = Y$. Denote an m-dimensional center manifold for (2.6) by $\mathcal{W}^c_{y,z}$, and let π be the restriction of π_y to $\mathcal{W}^c_{y,z}$.

Theorem 2.10.

(a) *The projection of the center subspace for the original network is the center subspace of the central network. That is,* $\pi_y(E^c_{y,z}) = E^c_y$.

(b) *The projection of a center manifold for the original network is a center manifold for the central network. That is,* $\mathcal{W}^c_y \equiv \pi(\mathcal{W}^c_{y,z})$ *is a center manifold for the central network equations* (2.6a).

(c) *The dynamics on the central network center manifold* $\mathcal{W}^c_y$ *are conjugate to the dynamics on the center manifold of the original network* $\mathcal{W}^c_{y,z}$.

Proof. Since all critical components are in the central network, $E^c_{y,z} \cap (\{0\} \times \mathbb{R}^{n_z}) = \{0\} \times \{0\}$. Hence, $(d\pi)_0 = \pi_y|_{E^c_{y,z}}$ is injective. Since $E^c_{y,z}$ and E^c_y have the same dimension, $\pi_y : E^c_{y,z} \to E^c_y$ is an isomorphism.

Injectivity of $(d\pi)_0$ implies that π is locally injective, so $\mathcal{W}^c_y \equiv \pi(\mathcal{W}^c_{y,z})$ is locally a submanifold. We claim that $\mathcal{W}^c_y$ is a center manifold for the central network. This is proved in two steps. First, we show that the tangent space of $\mathcal{W}^c_y$ at the origin is E^c_y. This follows from

$$T_0\mathcal{W}^c_y = T_0\pi(\mathcal{W}^c_{y,z}) = (d\pi)_0(T_0\mathcal{W}^c_{y,z}) = (d\pi)_0(E^c_{y,z}) = E^c_y,$$

where T_0 denotes the tangent space of a manifold at the origin.

Next, we show that $\mathcal{W}^c_y$ is flow-invariant under the vector field on the central network (2.6a). Let $\eta = (G, H)|_{\mathcal{W}^c_{y,z}}$ be the vector field (2.6) restricted to the chosen center manifold for the original network. By construction, the pushforward $\pi_*(\eta)$ leaves the submanifold $\mathcal{W}^c_y$ flow-invariant. By direct calculation, $\pi_*(\eta) = G|_{\mathcal{W}^c_y}$.

Let Ψ_t be the flow of the vector field η on the center manifold $\mathcal{W}^c_{y,z}$ for the original network. Let Φ_t be the flow of $\pi_*\eta$ on the center manifold $\mathcal{W}^c_y$ for the central network. By the definition of pushforward, $\Phi_t = \pi\Psi_t\pi^{-1}$, so Φ and Ψ are conjugate. ∎

2.3. Interpretation of results. In applications of networks of coupled dynamical systems, what matters most is not the abstract nature of the dynamics (steady, periodic, quasi-periodic, chaotic, and so on) of the entire system, but the dynamics of individual nodes. Indeed, a major feature that distinguishes network dynamics from general dynamical systems theory is the presence of distinguished node variables.

We sketch the implications of our results in terms of the dynamics of individual nodes of the network. The discussion can be placed in the context of pattern formation: what is the pattern of dynamic behavior, described from the viewpoint of the nodes?

We give a fairly complete answer (with proofs) for the codimension-1 bifurcations, steady-state, and Hopf. See Theorems 3.3 and 3.7. The result for Hopf bifurcation (all downstream nodes from the critical component oscillate) is consistent with the results in Golubitsky, Romano, and Wang (2010, 2012); Joly (2012). For the codimension-2 mode interactions considered in this paper, with two critical components, one being downstream from the other, we base our description on some plausible but sometimes unproved conjectures about the extent to which observing a single node can accurately reflect the dynamics of the system.

Filling in the details rigorously (and correcting them if necessary) offers much scope for future work. One feature of this paper deserves emphasis: the results apply to arbitrarily large (fully inhomogeneous) networks. Even when the number of nodes, and hence state variables, is large, the most likely bifurcations have low codimension; roughly speaking, the smaller the codimension, the more common the bifurcation is likely to be.

Our results show that typical mode interactions when one critical component is downstream from the other differ from the corresponding mode interactions in general dynamical systems. In a general system, a steady-state/steady-state (Takens–Bogdanov) mode interaction can create periodic solutions. A Hopf/steady-state mode interaction can lead to 2-tori. A Hopf/Hopf mode interaction can lead to 3-tori. Since a center manifold reduction captures all of the dynamics of the full system of ODEs near the bifurcation point, our analysis shows that these extra frequency motions do not occur when the critical components are related in

the feedforward manner assumed here.

This assertion follows from two principles. The main principle is heuristically reasonable: if a particular node A has a certain qualitative kind of dynamic behavior, then generically every node B downstream from A receives (either direct or indirectly) a signal from A. For example, if A oscillates periodically, then B receives an input with the same period. If the other inputs to B have dynamics similar to A, then B receives no other *conflicting* signals, so we expect B to oscillate periodically as well. (In effect, we can think of B as being "forced" by its inputs and consider the case where all inputs produce a consistent type of forcing. Steady inputs act like parameters and do not conflict with each other, nor with periodic ones.) Although effects such as resonance might cause the period of B to differ from that of A, these would normally require higher codimension behavior, so we ignore such possibilities here. In the case of a codimension-1 Hopf bifurcation, which creates a periodic state of the whole system, the period of B should be the same as that of A. For similar reasons, the growth rates of particular states along bifurcating branches in a codimension-1 steady-state bifurcation should also be the same for A and B.

Potential complications arise when B is downstream from both critical components because the incoming signals can interact. However, sufficiently close to the bifurcation point, solutions should be well described by appropriate linearized eigenfunctions, and this remark applies to the entire network. For example, if a node is forced by a periodic signal from the upstream critical component, and a quasi-periodic signal from the other component, these signals share a common frequency. This suggests that no node in the full network should exhibit more complicated dynamics than occurs in the normal form. In particular, steady states continue to act like parameters, so the difficult case is a Hopf-Hopf mode interaction. Generically, the two periods are incommensurable, so we expect B to behave quasi-periodically (invariant 2-torus) near the bifurcation point.

Consider first a codimension-1 bifurcation with critical component C. We partition nodes into two kinds: those downstream from C (including those in C) and the rest. Denote these sets of nodes by $\mathcal{D}$ and $\mathcal{R}$, respectively.

Nodes in $\mathcal{R}$ receive no signals from the critical components, so they do not "feel" the bifurcation. Our standing assumption is that bifurcation occurs from an equilibrium, which is hyperbolic away from the center subspace. Therefore nodes in $\mathcal{R}$ remain steady, and the implicit function theorem implies that when projected onto each such node, the equilibrium state moves smoothly with the bifurcation parameter λ. Thus the state of each node in $\mathcal{R}$ moves along a smooth path parametrized by λ, with typical growth rate $|\lambda|$.

Nodes in $\mathcal{D}$, on the other hand, do "feel" the bifurcation. Consider first a steady-state bifurcation. Since we prove that generically this is a saddle-node, we expect a bifurcation diagram resembling a saddle-node in each node of $\mathcal{D}$, so the growth rate is $\sqrt{|\lambda|}$ and the branch folds over on itself like a parabola. For a Hopf bifurcation, all nodes in $\mathcal{D}$ should begin to oscillate, with a common period (determined by the relevant conjugate pair of imaginary eigenvalues).

In the codimension-1 case, we can read off this behavior from the entries in a critical eigenvector, as in Theorem 3.3 for steady-state bifurcation and Theorem 3.7 for Hopf bifurcation. Thus we can make the above description rigorous in these cases.

We now come to codimension-2 mode interactions, with our standing assumption that one

critical component C_2 is downstream from the other C_1. Now we partition nodes into four disjoint subsets:

(a) Subset $\mathcal{R}$: Nodes not downstream from either C_1 or C_2.
(b) Subset $\mathcal{D}_1$: Nodes downstream from C_1 but not from C_2.
(c) Subset $\mathcal{D}_2$: Nodes downstream from C_2 (which must therefore be downstream from C_1).

The definition implies that each of these sets is a union of transitive components of the network. See Figure 1, where for simplicity the only transitive components with more than one node are C_1, C_2, and a set of three white nodes at the top of the figure.

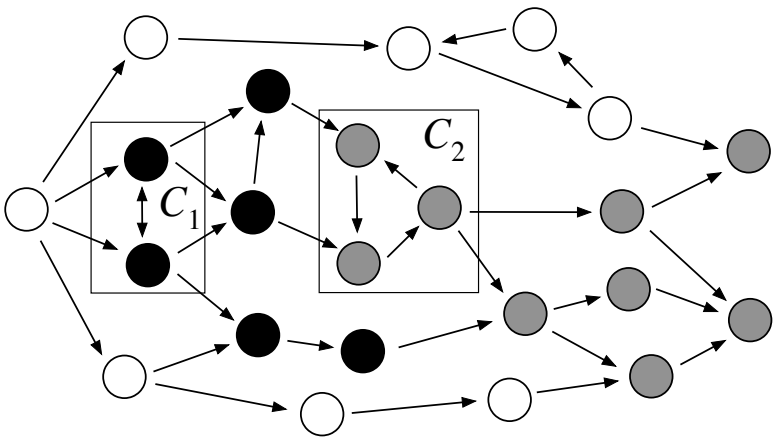

Figure 1. *Partition of a* 23*-node network into* 20 *transitive components and three disjoint subsets indicated by color. White:* $\mathcal{R}$*. Black:* $\mathcal{D}_1$*. Grey:* $\mathcal{D}_2$*.*

Now the (heuristic and unproved) principles that we assume govern the behavior are the following:

($\mathcal{R}$) Nodes in $\mathcal{R}$ are unaffected by the bifurcation. They thus remain in a steady state, with typical growth rate $|\lambda|$, because of the implicit function theorem.
($\mathcal{D}_1$) Nodes in $\mathcal{D}_1$ all have the same qualitative behavior. If C_1 is steady-state, the behavior is like the codimension-1 steady-state case. If C_1 is Hopf, the behavior is like the codimension-1 Hopf case.
($\mathcal{D}_2$) Nodes in $\mathcal{D}_2$ all have the same qualitative behavior. This is described by the C_2-component of the appropriate normal form. Based on Theorem 2.10(c), the behavior of all nodes in $\mathcal{D}_2$ is identical to those in C_2, independently of whether the nodes receive a direct signal from the C_1-component or not.

Typically, in general systems of differential equations, universal unfoldings of codimension-2 mode interactions lead to solutions with additional frequencies. For example, Takens–Bogdanov singularities can perturb to periodic solutions and steady-state/Hopf mode interactions can lead to two frequency solutions. However, we show that solutions with these additional frequencies are not to be expected in network mode interaction unfoldings. This is a (perhaps surprising) expectation based on the theorems stated in section 5. These statements are consistent with the simulations of the example discussed in section 2.4B.

For any given node in $\mathcal{D}_1$ or $\mathcal{D}_2$, the growth rate is expected to be the same as that given

by the normal form for any specific branch. We do not expect anomalous growth rates of the kind discussed in Stewart and Golubitsky (2011); Stewart (2014) for steady-state bifurcation and Elmhirst and Golubitsky (2006); Golubitsky and Postlethwaite (2012) for Hopf bifurcation because the networks concerned are homogeneous. (Also, in the steady-state case, they are highly artificial, with a small number of nodes connected by arrows with large multiplicities.)

To summarize, our general results make it possible (conjecturally but plausibly) to predict the general type of dynamic behavior on each node of the network: whether it is steady, periodic, or quasi-periodic; how the periods concerned are related; and the growth rate of any particular branch. The ingredients for the prediction are the type of mode interaction and the associated singularity-theoretic normal form.

In any specific model, the components of the critical eigenvectors add further quantitative information. For example, when Hopf bifurcation is involved, these components determine the initial relative amplitudes and phases of the bifurcating branches. As observed earlier, the interpretation of our results for the behavior of individual nodes can be viewed as a description of the types of dynamic pattern formation that are associated with codimension-1 and codimension-2 bifurcations of the feedforward type considered in this paper.

2.4. Examples. This subsection presents three types of examples that should help the reader understand our results. In section 2.4A, we present two large regulatory networks that have appeared in the literature (Tyson and Novak (2010); Chen et al. (2019)). In section 2.4B, we illustrate how patterns of oscillation appear in a moderate sized network with multiple path components. In section 2.4C, we discuss our results in the context of four three-node network motifs that are common in networks, as discussed in Milo et al. (2002); Tyson and Novak (2010).

A. Sample real-world networks. Information processing of a living cell is determined by complex networks of interacting genes and proteins of the type we consider in this paper (see Figures 2 and 3). Such systems are examples of fully inhomogeneous networks consisting of distinct types of nodes (proteins and genes). These networks are modeled by admissible systems of ODEs as described below for the network in Figure 2. Such networks frequently have a feedforward structure. Figure 3 (right) illustrates the decomposition of the left network into path components.

Tyson and Novak (2010) model the network in Figure 2 using ODEs of the form

$$\dot{X}_i = \gamma_i \frac{A_i(1 - X_i) - B_i X_i}{A_i + B_i}, \quad i = 1, \dots, N, \tag{2.7}$$

where the state variable X_i is the action fraction of the ith protein, and A_i and B_i are raw rates of activation and inhibition of protein X_i. These rates depend on other nodes in the network that are directly connected to node i. See Tyson and Novak (2010) for function forms of the raw rates.

To understand the information processing ability of a living cell, Tyson and Novak (2010) identify basic functional motifs in the protein regulatory network and use ODEs (2.7) to explore the qualitative dynamical features of these motifs. One basic motif in Figure 2 is a feedback loop (network 1 in Figure 10); for example, Casp3 $\to$ Casp6 $\to$ Casp8 $\to$ Casp3, which implies that the three nodes concerned must be in the same path component. Another

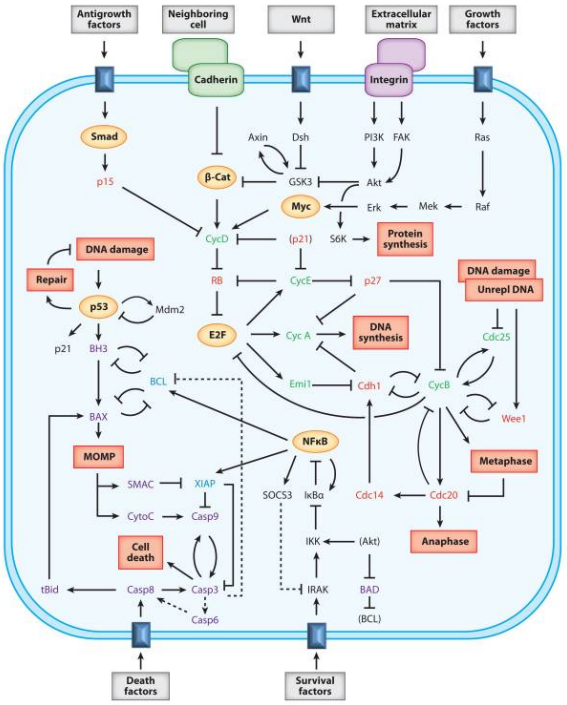

Figure 2. *An example of a protein regulatory network from* Tyson and Novak (2010). *Yellow ovals and text of other colors indicate proteins, and arrows indicate interactions between proteins. Reprinted with permission from Annual Reviews, Inc.*

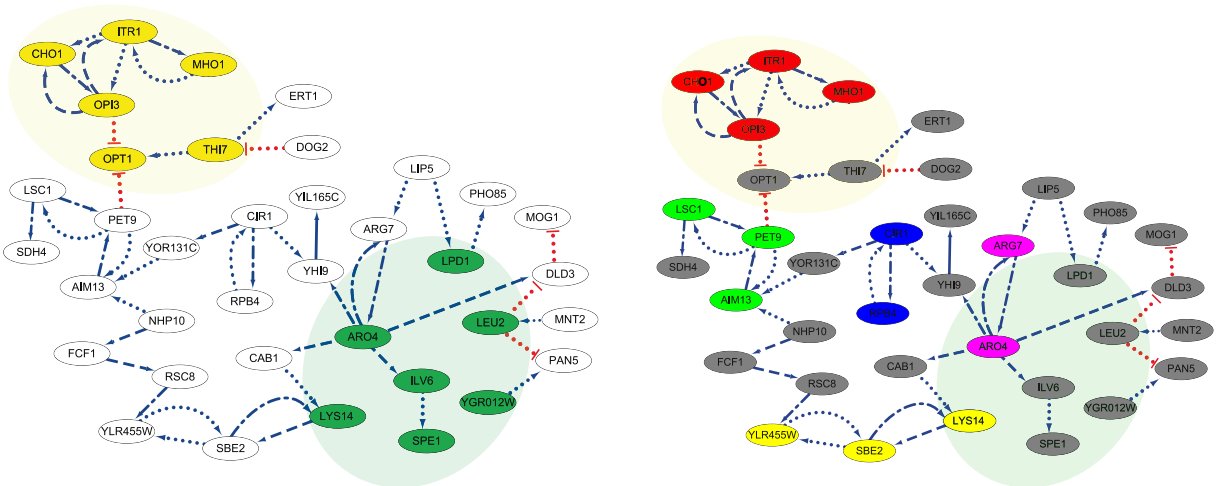

Figure 3. *Ovals indicate genes or proteins, and arrows indicate interactions.* (Left) *An example of a yeast gene regulatory network from* Chen et al. (2019). *Reproduced with permission from the authors.* (Right) *Path components of the network on the left. Gray nodes are components consisting of single nodes; other colors are multiple node components.*

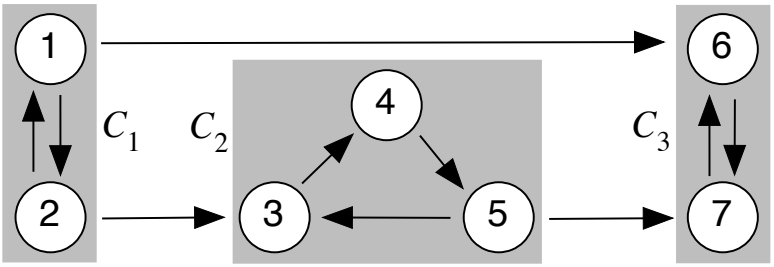

Figure 4. *Network with seven nodes and three transitive components (shaded rectangles).*

common motif in regulatory networks is a feedforward chain (network 2 in Figure 10). For example, the transcription factor (Smads) stimulates the production of response proteins (p15), which inhibits CycD. The feedforward loop among proteins E2F, Emi1, Cdh1, and CycA is also a prevalent motif, the prototype of which is network 3 in Figure 10.

B. Hopf bifurcations in a seven-node network with three path components. Using the network illustrated in Figure 4, we present four simulations (see Table 1): one simulation near a Hopf bifurcation associated with each of the three path components (Figures 5–7) and one simulation near a Hopf/Hopf mode interaction where path components C_1 and C_2 are critical (Figure 8). The simulations are performed on the three parameter admissible system (2.8). Each parameter is associated with a Hopf bifurcation in one of the path components.

Table 1

Four predicted patterns of oscillation: S = steady-state, P = periodic oscillation, T = two-frequency oscillation; on = unstable eigenvalues, off = stable eigenvalues.

Case	$\{1,2\}$	$\{3,4,5\}$	$\{6,7\}$	1	2	3	4	5	6	7
1	on	off	off	P	P	P	P	P	P	P
2	off	on	off	S	S	P	P	P	P	P
3	off	off	on	S	S	S	S	S	P	P
4	on	on	off	P	P	T	T	T	T	T

We assume all nodes have phase space $\mathbb{R}$, our system has a trivial equilibrium at the origin, and for each component the Hopf bifurcation occurs at the origin. Specifically, we consider the following family of admissible ODEs:

$$
\begin{aligned}
\dot{x}_1 &= f_1(x_1,x_2) &&= a_1x_1 - x_2 - 0.1x_1(x_1^2+x_2^2),\\
\dot{x}_2 &= f_2(x_1,x_2) &&= 2x_1 + a_1x_2 - 0.1x_2(x_1^2+x_2^2),\\
\dot{x}_3 &= f_3(x_2,x_3,x_5) &&= -x_3 - 0.01x_3^3 - 3x_5 + 2x_2,\\
\dot{x}_4 &= f_4(x_3,x_4) &&= -2x_4 - 0.01x_4^3 + c_{43}x_3,\\
\dot{x}_5 &= f_5(x_4,x_5) &&= -x_5 - 0.01x_5^3 - x_4,\\
\dot{x}_6 &= f_6(x_1,x_6,x_7) &&= a_6x_6 - \sqrt{2}x_7 - 0.1x_6(x_6^2+x_7^2) + 0.1x_1,\\
\dot{x}_7 &= f_7(x_5,x_6,x_7) &&= \sqrt{2}x_6 + a_6x_7 - 0.1x_7(x_6^2+x_7^2) + 0.5x_5
\end{aligned}
\tag{2.8}
$$

with internal parameter a_1 for transitive component $C_1 = \{1,2\}$, internal parameter c_{43} for transitive component $C_2 = \{3,4,5\}$, and internal parameter a_6 for transitive component $C_3 = \{6,7\}$.

The Jacobian of (2.8) at the equilibrium at the origin is

$$J = \left[\begin{array}{cc|ccc|cc} a_1 & -1 & 0 & 0 & 0 & 0 & 0 \\ 2 & a_1 & 0 & 0 & 0 & 0 & 0 \\ \hline 0 & 2 & -1 & 0 & -3 & 0 & 0 \\ 0 & 0 & c_{43} & -2 & 0 & 0 & 0 \\ 0 & 0 & 0 & -1 & -1 & 0 & 0 \\ \hline 0.1 & 0 & 0 & 0 & 0 & a_6 & -\sqrt{2} \\ 0 & 0 & 0 & 0 & 0.5 & \sqrt{2} & a_6 \end{array}\right]. \tag{2.9}$$

Note that $a_1 = 0$ leads to a Hopf bifurcation in component C_1 and $a_6 = 0$ leads to a Hopf bifurcation in component C_3. Less obviously, the linearized coupling $c_{43} = 6$ leads to a Hopf bifurcation in path component C_2. This value is obtained using Lemma 2.11.

Lemma 2.11. *Let*

$$J_2 = \begin{bmatrix} \alpha_1 & 0 & \beta_1 \\ \beta_2 & \alpha_2 & 0 \\ 0 & \beta_3 & \alpha_3 \end{bmatrix}$$

be the Jacobian of the second path component of the network in Figure 4. Let

$$\begin{array}{rcl} A_1 & = & \alpha_1 + \alpha_2 + \alpha_3, \\ A_2 & = & \alpha_1\alpha_2 + \alpha_1\alpha_3 + \alpha_2\alpha_3, \\ A_3 & = & \alpha_1\alpha_2\alpha_3 + \beta_1\beta_2\beta_3. \end{array} \tag{2.10}$$

Then the eigenvalues of J_2 are $\gamma < 0$ and a pair $\pm\omega i$ if and only if $A_1 < 0$, $A_2 > 0$ and

$$A_3 = A_1 A_2.$$

Specifically,

$$\gamma = A_1 < 0 \quad \textit{and} \quad \omega^2 = A_2 > 0.$$

Proof. The characteristic polynomial of J_2 is

$$\det(\lambda I_3 - J_2) = \det \begin{bmatrix} \lambda - \alpha_1 & 0 & -\beta_1 \\ -\beta_2 & \lambda - \alpha_2 & 0 \\ 0 & -\beta_3 & \lambda - \alpha_3 \end{bmatrix} = \lambda^3 - A_1\lambda^2 + A_2\lambda - A_3.$$

The eigenvalues of J_2 are γ and $\pm\omega i$ if and only if

$$\lambda^3 - A_1\lambda^2 + A_2\lambda - A_3 = (\lambda - \gamma)(\lambda^2 + \omega^2) = \lambda^3 - \gamma\lambda^2 + \omega^2\lambda - \gamma\omega^2.$$

Therefore, $\gamma = A_1 < 0$, $\omega^2 = A_2 > 0$, and $\gamma\omega^2 = A_3 < 0$. Hence, $A_3 = A_1 A_2$, as claimed. ∎

In the admissible system (2.8), we have

$$\begin{array}{rcll} A_1 & = & -1 - 2 - 1 & = & -4, \\ A_2 & = & (-1)(-2) + (-1)(-1) + (-2)(-1) & = & 5, \\ A_3 & = & (-1)(-2)(-1) + (-3)c_{43}(-1) & = & 3c_{43} - 2. \end{array}$$

Observe that Hopf bifurcation occurs in C_2 when $A_3 = A_1A_2 = -20$, that is, when $a_{43} = -6$.

The simulations show that all nodes oscillate with the same frequency after a C_1 Hopf bifurcation; nodes 3–7 oscillate with the same frequency after a C_2 Hopf bifurcation, and nodes 6–7 oscillate with the same frequency after a C_3 Hopf bifurcation. As with Hopf-Hopf mode interactions in standard bifurcation theory, the results near a C_1-C_2 Hopf-Hopf mode interaction are complicated to predict exactly. Since component C_2 is downstream from component C_1, one solution type has nodes 1–2 oscillating periodically and nodes 3–7 oscillating with a two-frequency motion, as predicted by Theorem 2.10(c) and as confirmed heuristically by plotting the attractor. Such a solution type is illustrated in Figure 8 with the torus illustrated in Figure 9.

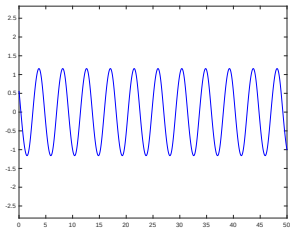

(a) C_1 Hopf; Node 1

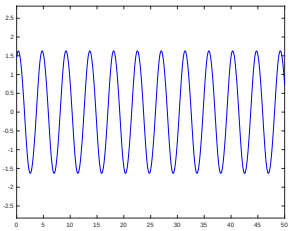

(b) C_1 Hopf; Node 2

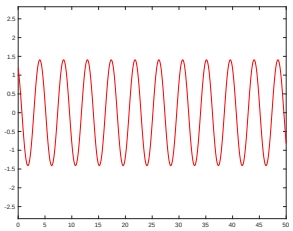

(c) C_1 Hopf; Node 3

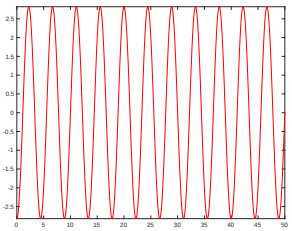

(d) C_1 Hopf; Node 4

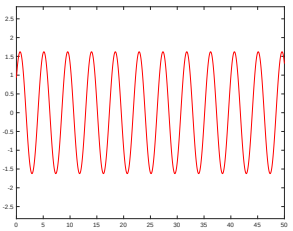

(e) C_1 Hopf; Node 5

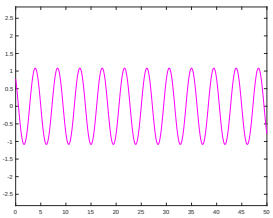

(f) C_1 Hopf; Node 6

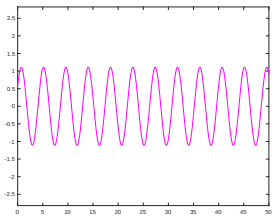

(g) C_1 Hopf; Node 7

Figure 5. *Case* 1*: Oscillation pattern in C_1 Hopf bifurcation using* (2.8)*. All nodes oscillate with the same frequency. The ordinates in each subfigure are identical so that the relative nodal amplitudes can be observed. Parameters:* $a_1 = 0.2, c_{43} = -5.0, a_6 = -0.3$.

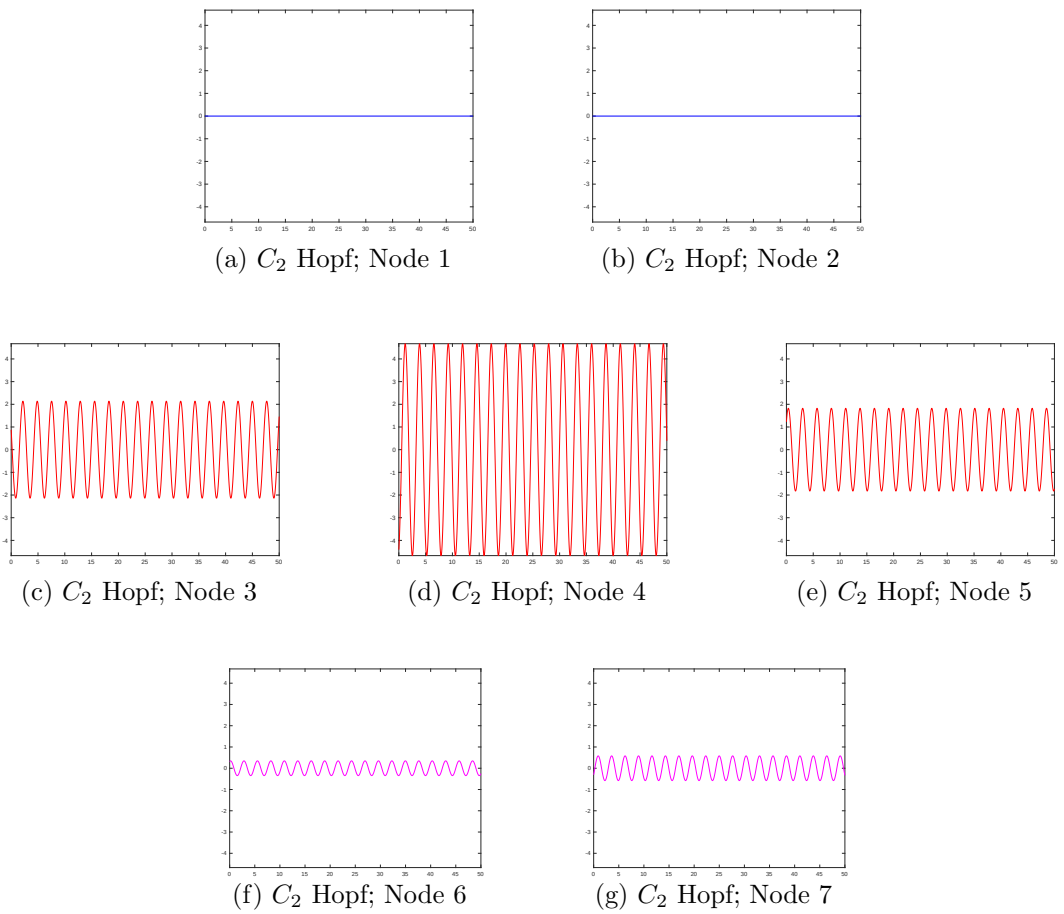

(a) C_2 Hopf; Node 1 (b) C_2 Hopf; Node 2

(c) C_2 Hopf; Node 3 (d) C_2 Hopf; Node 4 (e) C_2 Hopf; Node 5

(f) C_2 Hopf; Node 6 (g) C_2 Hopf; Node 7

Figure 6. *Case 2: Oscillation pattern in C_2 Hopf bifurcation using (2.8). Nodes 3–7 oscillate with the same frequency; nodes 1–2 are quiescent. The ordinates in each subfigure are identical so that the relative nodal amplitudes can be observed. Parameters: $a_1 = -0.2, c_{43} = -7.0, a_6 = -0.3$.*

C. Three-node motif networks. Most results in this paper are independent of the number of nodes in the network. However, here we use a selection of three-node inhomogeneous networks to illustrate how network structure can influence dynamics by restricting the types of bifurcations that are possible.

We note that up to relabeling there are 13 possible connected three-node inhomogeneous networks (Harary (1994); Tyson and Novak (2010); Golubitsky and Wang (2019)). Five are transitive (that is, do not have feedforward structure), and eight have feedforward structure. Figure 10 contains four three-node network diagrams: (1) the *feedback loop*, (2) the *feedforward chain*, (3) the *feedforward loop*, and (4) the *downlinked dyad*. In each case, we discuss the role network structure plays in restricting the bifurcations that are possible. Table 2 provides

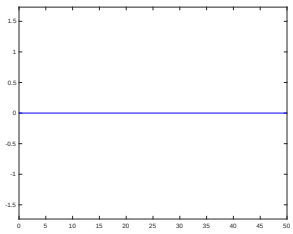

(a) C_3 Hopf; Node 1

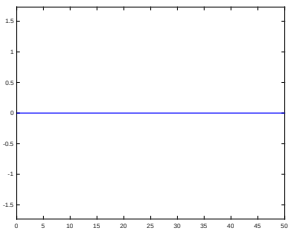

(b) C_3 Hopf; Node 2

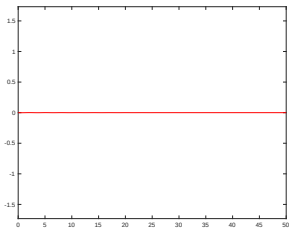

(c) C_3 Hopf; Node 3

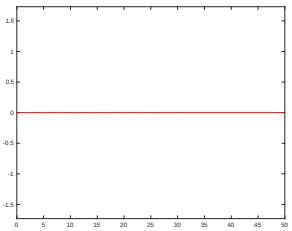

(d) C_3 Hopf; Node 4

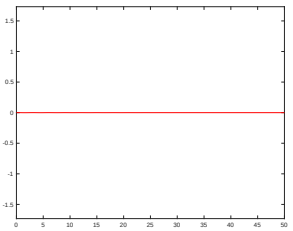

(e) C_3 Hopf; Node 5

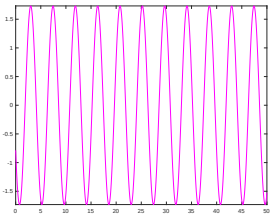

(f) C_3 Hopf; Node 6

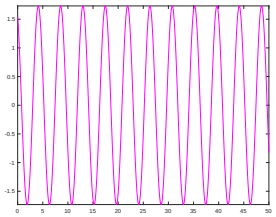

(g) C_3 Hopf; Node 7

Figure 7. *Case* 3*: Oscillation pattern in* C_3 *Hopf bifurcation using* (2.8)*. Nodes* 6–7 *oscillate with the same frequency; nodes* 1–5 *are quiescent. The ordinates in each subfigure are identical so that the relative nodal amplitudes can be observed. Parameters:* $a_1 = -0.2, c_{43} = -5.0, a_6 = 0.3$.

a summary of the possible codimension-1 bifurcations and codimension-2 mode interactions that are possible for admissible dynamical systems in these networks. Note that the three-dimensional phase space associated with these networks makes Hopf/Hopf mode interaction impossible in all cases. Using Milo et al. (2002), we highlight application areas where these networks have been noted as subnetwork motifs that appear frequently in larger networks.

Network 1. The feedback loop consists of a single path component and often appears in electronic circuits. The codimension-1 steady-state and Hopf bifurcations in this network are generically of the same type as those observed in a general three-dimensional dynamical system.

Surprisingly, no steady-state/Hopf mode interaction can occur in an admissible dynamical

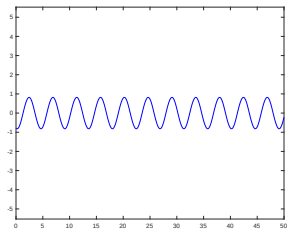

(a) $C_{1,2}$ Hopf/Hopf; Node 1

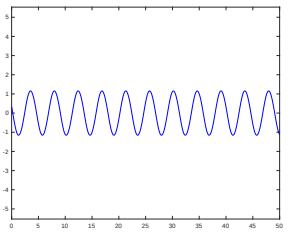

(b) $C_{1,2}$ Hopf/Hopf; Node 2

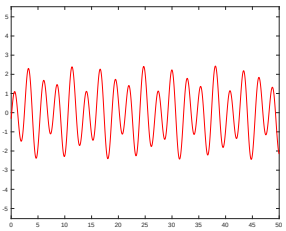

(c) $C_{1,2}$ Hopf/Hopf; Node 3

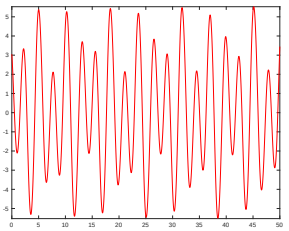

(d) $C_{1,2}$ Hopf/Hopf; Node 4

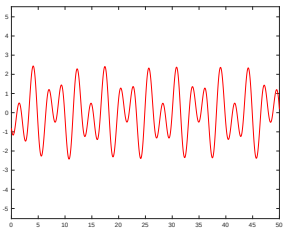

(e) $C_{1,2}$ Hopf/Hopf; Node 5

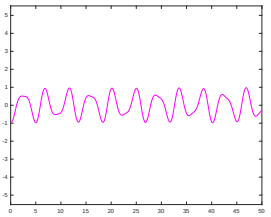

(f) $C_{1,2}$ Hopf/Hopf; Node 6

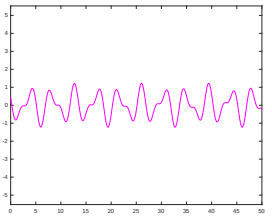

(g) $C_{1,2}$ Hopf/Hopf; Node 7

Figure 8. *Case* 4*: Oscillation pattern in mixed-mode C_1 Hopf/C_2 Hopf bifurcation using* (2.8)*. Nodes* 1–2 *oscillate with the same frequency; nodes* 3–7 *oscillate with two frequencies. The ordinates in each subfigure are identical so that the relative nodal amplitudes can be observed. Parameters:* $a_1 = 0.1, c_{43} = -7.0, a_6 = -0.3$.

system in a feedback loop. First, observe that the Jacobian J of a network admissible system has the form (2.10). Lemma 2.11 implies that if J has eigenvalues 0 and $\pm\omega i$, then

$$A_1 = \alpha_1 + \alpha_2 + \alpha_3 = 0 \quad \text{and} \quad A_2 = \alpha_1\alpha_2 + \alpha_1\alpha_3 + \alpha_2\alpha_3 > 0.$$

It follows that

$$\alpha_3 = -\alpha_1 - \alpha_2 \quad \text{and} \quad A_2 = \alpha_1\alpha_2 - (\alpha_1 + \alpha_2)^2 = -(\alpha_1^2 + \alpha_1\alpha_2 + \alpha_2^2) \leq 0,$$

which is a contradiction.

Steady-state/steady-state mode interactions can occur in the feedback loop. Generically the resulting bifurcation is a standard codimension-2 Takens–Bogdanov bifurcation. We will

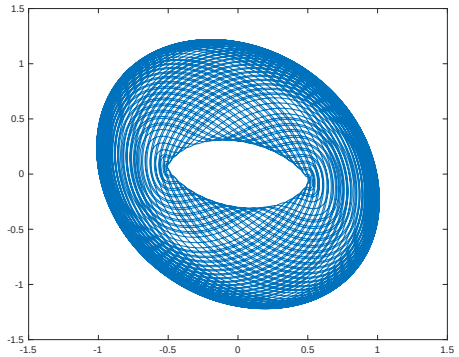

Figure 9. *Torus in Case* 4 *illustrated by plotting* x_6 *versus* x_7.

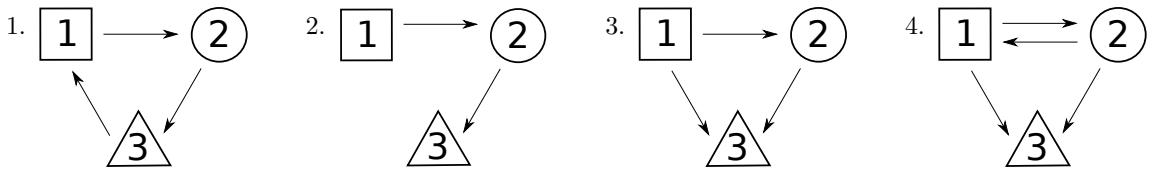

Figure 10. *The figures show four examples of inhomogeneous three-node networks:* (1) *feedback loop,* (2) *feedforward chain,* (3) *feedforward loop, and* (4) *downlinked dyad. Each node is assumed to be one-dimensional.*

Table 2

Number of path components and possible distinct bifurcations for the networks given in Figure 10*:* (1) *feedback loop,* (2) *feedforward chain,* (3) *feedforward loop, and* (4) *downlinked dyad. The distinct codimension-*1 *steady-state and Hopf bifurcations are each associated with a single path component. Each of the two critical path components in the four mode interactions can be associated with either a steady-state or Hopf bifurcation. The number of possible mode interactions in distinct path components is indicated. Because of dimension restrictions in these examples, the only mode interactions that can appear within a single path component are of Takens–Bogdanov type.*

	(1) FBL	(2) FFC	(3) FFL	(4) DLD
Path components	1	3	3	2
Steady-state (SS)	1	3	3	2
Hopf (H)	1	0	0	1
Takens–Bogdanov	1	0	0	1
SS/SS	0	3	3	2
H/SS	0	0	0	1
SS/H	0	0	0	0
H/H	0	0	0	0

not verify this point here. Since the feedback loop has one path component, the steady-state/steady-state mode interactions that we analyze in this paper are not relevant for this network.

Network 2. The feedforward chain is common within food webs and consists of three path components, each with one-dimensional phase space. The network structure therefore prohibits Hopf bifurcation, and only steady-state bifurcations are possible. There are three codimension-1 steady-state bifurcations, each associated with a different node and each exhibiting a distinct pattern of dynamics when projected onto the network nodes. Feedforward steady-state/steady-state mode interactions of the type discussed in section 5.1 also appear generically for admissible systems on this network.

Network 3. The feedforward loop is obtained by adding one arrow to Network 2. It is a prevalent motif in gene regulatory networks, neural networks, and electronic circuits. The center manifold dynamics for all possible bifurcations that generically appear in this network are isomorphic to those of Network 2. See Theorem 2.10. It is in this sense that we claim that there is no difference between bifurcation types in the feedforward chain and the feedforward loop.

Network 4. The downlinked dyad is obtained by adding one arrow to Network 3. In this case, the additional connection plays a crucial role in the appearance of distinctly different generic bifurcations. Network 4 consists of two path components, a two-node component that sends input to a one-node component. Hopf bifurcation is possible and can be associated with the upstream path component. This also allows for feedforward H/SS mode interactions of the type discussed in section 5.2. In addition, both a feedforward steady-state/steady-state mode interaction and a standard Takens–Bogdanov mode interaction associated with the upstream path component are allowed by the network structure.

The H/SS mode interaction associated with Network 4 has an interesting dynamical feature: an invariant cylinder. See Remark 5.13. To exemplify this result, we consider the admissible system

$$\begin{aligned} \dot{x} &= \lambda x + y - (x^2 + 3y^2)x, \\ \dot{y} &= -2x + \lambda y - (x^2 + y^2)y, \\ \dot{z} &= \varepsilon\big(\mu - z^2 + 10y - (0.1x^2 + y^2)\big) \end{aligned} \tag{2.11}$$

that exhibits a Hopf/steady-state mode interaction when $\lambda = \mu = 0$. The robust invariant cylinder is pictured in Figure 11 (left) with its cross-section shown in Figure 11 (right). In order to help visualize how trajectories approach the cylinder, we have taken the time scale $\varepsilon = 0.01$.

3. Codimension-1 bifurcations.

We prove that for codimension-1 bifurcations, the eigenvalues at bifurcation are simple and the central network is always a single critical path component. The proof that the eigenvalues are simple requires careful analysis, discussed in Theorem SM1.1 and Corollary SM1.2. The nonlinear analysis is described in two distinct cases: steady-state (section 3.1) and Hopf (section 3.2).

3.1. Codimension-1 steady-state bifurcations.

In section SM1.2, we prove two generic results about codimension-1 steady-state bifurcations of admissible differential equations, stated here as Theorems 3.1 and 3.3. First, these bifurcations are saddle-node; second, the

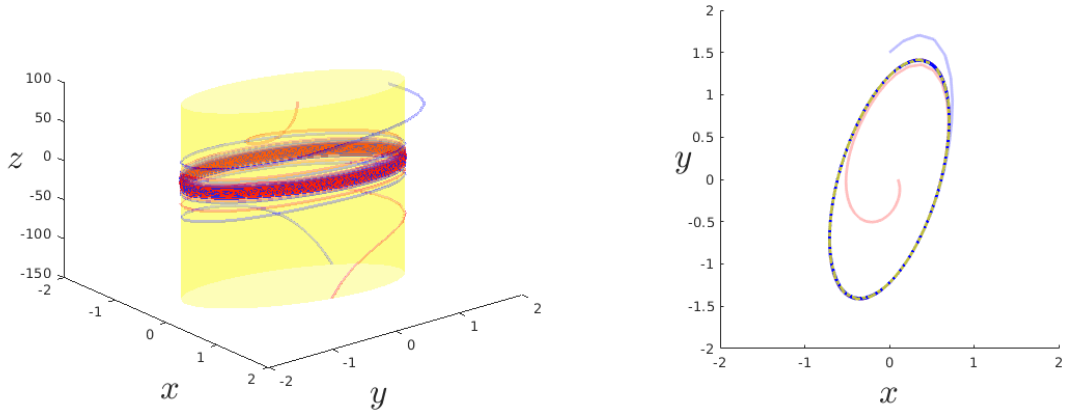

Figure 11. *Trajectories approach the invariant cylinder (yellow) from both inside (red) and outside (blue).* (Left) *Projection onto* (x, y, z) *phase space and* (right) *projection onto* (x, y) *plane. We have taken* $\lambda = 1$, $\varepsilon = 0.01$, $\mu = -1$.

growth rate of the equilibrium solution when viewed within any particular node is determined by the network architecture.

Theorem 3.1. *Generically, codimension-*1 *steady-state bifurcations on a fully inhomogeneous network are saddle-node bifurcations.*

Remark 3.2.

(a) The curve of equilibria emanating from a saddle-node bifurcation is tangent to the eigenvector v of the Jacobian at the bifurcation point. In particular, if a coordinate in v is nonzero, and assuming without loss of generality that the bifurcation occurs at $\lambda = 0$, then the growth rate of the zeros in that coordinate is of order $\sqrt{|\lambda|}$, where λ is the bifurcation parameter.

(b) This result is not always valid for networks that are not fully inhomogeneous, that is, where some arrows or nodes have the same type. The case of regular networks (all nodes and arrows are identical, and each node has the same number of input arrows) is discussed in Leite and Golubitsky (2006); Stewart and Golubitsky (2011); Stewart (2014).

Theorem 3.3. *Assume the bifurcation occurs at* $\lambda = 0$. *For all nodes within the critical path component, or nodes downstream from those, the growth rate of the equilibrium is* $\sqrt{|\lambda|}$. *The growth rate is at most* $|\lambda|$ *in all other components.*

Remark 3.4. It follows from Theorems 3.1 and 3.3 that generically the two solutions bifurcating from the saddle-node bifurcation have different coordinates on all nodes downstream from the critical components and the same values on all other nodes. In this sense, there is a pattern hidden in the bifurcation based on which component is the critical component.

3.2. Codimension-1 Hopf bifurcations. In section SM1.3, we prove two generic results about codimension-1 Hopf bifurcations of admissible differential equations for a fully inhomogeneous network, stated here as Theorems 3.6 and 3.7.

Definition 3.5. *The system* $\dot{X} = F(X, \lambda)$ *has a* nondegenerate *Hopf bifurcation at the equilibrium* X_0 *if the following hold:*

(a) *The Jacobian* $J = (d_X F)_{X_0,\lambda_0}$ *has a complex conjugate pair of simple purely imaginary eigenvalues with all other eigenvalues off of the imaginary axis.*

(b) *The growth rate of the small amplitude periodic solutions is* $\sqrt{\lambda}$.

The two theorems show that codimension-1 Hopf bifurcations are nondegenerate, and only the nodes downstream from a critical path component experience periodic motion.

Theorem 3.6. *Generically, codimension-*1 *Hopf bifurcation on a fully inhomogeneous network is nondegenerate.*

Theorem 3.7. *Hopf bifurcation yields periodic motion in all nodes in the critical path component* H *and any node downstream from* H. *The amplitude of this periodic motion has growth rate* $\sqrt{|\lambda|}$. *All other nodes remain constant and experience at most* $|\lambda|$ *growth rate.*

Remark 3.8. By Theorem 3.7, there is a unique type of Hopf bifurcation associated with each path component that can be critical, in the sense that the Jacobian on that path component can have imaginary eigenvalues. (This would not be possible, for example, if the component has a single node with one-dimensional phase space.) Theorem 3.7 implies that the type of Hopf bifurcation defines the set of nodes that generically oscillate. More specifically, bifurcating periodic solutions generically oscillate on all nodes downstream from the critical component and are constant on all other nodes.

4. Center manifolds for codimension-2 bifurcations. There are three possible central networks for codimension-2 bifurcations: (1) a single critical path component, (2) two disconnected critical path components, and (3) two critical path components with one strictly downstream of the other and possibly nodes in between. As stated in the introduction, we focus on case (3).

For case (3), suppose the network has two critical path components C_1 and C_3, with C_3 downstream from C_1. Let C_2 be the path components that are downstream from C_1 and upstream from C_3. Theorem 2.10 states that the center manifold dynamics of the original network is conjugate to the center manifold dynamics of the central network. That is, we can work with admissible vector fields on the central network that take the general form

$$\dot{x}_1 = f_1(x_1), \tag{4.1a}$$

$$\dot{x}_2 = f_2(x_1, x_2), \tag{4.1b}$$

$$\dot{x}_3 = f_3(x_1, x_2, x_3). \tag{4.1c}$$

Here $x_1 \in \mathbb{R}^{m_1}$, $x_2 \in \mathbb{R}^{m_2}$, and $x_3 \in \mathbb{R}^{m_3}$ are coordinates for the nodes in C_1, C_2, and C_3, respectively. By assumption, $f_1(0) = f_2(0,0) = f_3(0,0,0) = 0$. Throughout, we write $\mathrm{D}f$ for the derivative of a map f and $\mathrm{D}_j f$ for the partial derivative with respect to the jth variable. Sometimes we also denote the relevant variable by a subscript, as in $\mathrm{D}_x f$, which is $\partial f/\partial x$. The linearization about 0 is

$$J = \begin{bmatrix} J_1 & 0 & 0 \\ \mathrm{D}_1 f_2 & J_2 & 0 \\ \mathrm{D}_1 f_3 & \mathrm{D}_2 f_3 & J_3 \end{bmatrix},$$

where both $J_1 = \mathrm{D}f_1(0)$ and $J_3 = \mathrm{D}_3 f_3(0,0,0)$ have critical eigenvalues, whereas $J_2 = \mathrm{D}_2 f_2(0,0)$ is nonsingular. In section 2.3, we discussed how the dynamics on the central network affects non-central network nodes. We show that the flow restricted to the center manifold of (4.1) has a feedforward structure and depends only on the two critical components. This is proved in Theorem 4.3, but first we need two lemmas. The following three results are analogous to those proved in Golubitsky and Postlethwaite (2012).

Lemma 4.1. *The flow of* (4.1) *can be written as*

$$\Phi_t(x_1, x_2, x_3) = (\phi_{1t}(x_1), \phi_{2t}(x_1, x_2), \phi_{3t}(x_1, x_2, x_3)).$$

Proof. The feedforward structure of (4.1) implies that the flow of x_1 is independent of x_2 and x_3, and the flow of x_2 is independent of x_3. ∎

Assume that the center subspaces of J_1 and J_3 are the n_1-dimensional subspace E_1^c and the n_3-dimensional subspace E_3^c, respectively. Let $\pi_1(x_1, x_2, x_3) = (x_1, 0, 0)$ be projection onto the first coordinate; that is, $\pi_1 : \mathbb{R}^{m_1} \times \mathbb{R}^{m_2} \times \mathbb{R}^{m_3} \to \mathbb{R}^{m_1} \times \{0\} \times \{0\}$.

Let $\nu_1^c \times \{0\} \times \{0\}$ be an n_1-dimensional center manifold of (4.1a) in $\mathbb{R}^{m_1} \times \{0\} \times \{0\}$. It follows from Lemma 4.1 and the fact that ν_1^c is flow-invariant for (4.1a) that $\pi_1^{-1}(\nu_1^c \times \{0\} \times \{0\}) = \nu_1^c \times \mathbb{R}^{m_2} \times \mathbb{R}^{m_3}$ is flow-invariant for (4.1). Therefore we can choose an $(n_1 + n_3)$-dimensional center manifold $\mathcal{W}^c$ for (4.1) in $\pi_1^{-1}(\nu_1^c \times \{0\} \times \{0\})$ such that $\pi_1(\mathcal{W}^c) = \nu_1^c \times \{0\} \times \{0\}$.

Let ν_3^c be an n_3-dimensional center manifold of (4.1c) on $x_1 = x_2 = 0$. Since (4.1a)–(4.1b) have 0 as fixed point, $\{0\} \times \{0\} \times \nu_3^c$ is flow-invariant. We can choose $\mathcal{W}^c$ so that

$$\{0\} \times \{0\} \times \nu_3^c \subseteq \mathcal{W}^c$$

is a submanifold.

Lemma 4.2. *The manifold $\nu_1^c \times \{0\} \times \{0\}$ is a submanifold of $\mathcal{W}^c$, and $\mathcal{W}^c$ is a fiber bundle over the base $\nu_1^c \times \{0\} \times \{0\}$ with fibers diffeomorphic to $\{0\} \times \{0\} \times \nu_3^c$.*

Proof. First, we show that

$$\nu_1^c \times \{0\} \times \{0\} \subseteq \mathcal{W}^c$$

by verifying that

$$\nu_1^c \times \{0\} \times \{0\} = \mathcal{W}^c \cap (\mathbb{R}^{m_1} \times \{0\} \times \{0\}).$$

To this end, we define

$$\hat{\nu}_1^c = \mathcal{W}^c \cap (\mathbb{R}^{m_1} \times \{0\} \times \{0\})$$

and note that $\hat{\nu}_1^c$ is an n_1-dimensional manifold. Indeed, the center manifold theorem lets us coordinatize the center manifold $\mathcal{W}^c$ of the network by its center subspace E^c. Now $\hat{\nu}_1^c$ is the slice of $\mathcal{W}^c$ along the direction that contains the n_1-dimensional subspace E_1^c, so $\dim(\hat{\nu}_1^c) = n_1$.

Moreover, π_1 is the identity on $\mathbb{R}^{m_1} \times \{0\} \times \{0\}$, so $\pi_1(\hat{\nu}_1^c) = \hat{\nu}_1^c$. Therefore

$$\begin{aligned} \hat{\nu}_1^c &= \pi_1(\mathcal{W}^c \cap (\mathbb{R}^{m_1} \times \{0\} \times \{0\})) \\ &\subseteq \pi_1(\mathcal{W}^c) \cap \pi_1((\mathbb{R}^{m_1} \times \{0\} \times \{0\})) \\ &= (\nu_1^c \times \{0\} \times \{0\}) \cap ((\mathbb{R}^{m_1} \times \{0\} \times \{0\})) \\ &= \nu_1^c \times \{0\} \times \{0\}. \end{aligned} \tag{4.2}$$

Since $\hat{\nu}_1^c$ and $\nu_1^c \times \{0\} \times \{0\}$ are manifolds with the same dimension, they must be the same, so $\nu_1^c \times \{0\} \times \{0\} \subseteq \mathcal{W}^c$.

Second, choose $z_1 \in \nu_1^c$. Write $\mathcal{W}^c$ as a fiber bundle with base $\nu_1^c \times \{0\} \times \{0\}$. For each z_1, define the fiber over z_1 as

$$\mathcal{U}_{z_1} = \mathcal{W}^c \cap (\{z_1\} \times \mathbb{R}^{m_2} \times \mathbb{R}^{m_3}) = \{z \in \mathcal{W}^c : \pi_1(z) = (z_1, 0, 0)\}.$$

Thus, $\mathcal{U}_{z_1}$ is diffeomorphic to $\mathcal{U}_0$, where $\mathcal{U}_0 = \{0\} \times \{0\} \times \nu_3^c$. ∎

In coordinates on the $(n_1 + n_2)$-dimensional fiber bundle $\mathcal{W}^c$, we have proved that we can choose a fiber-preserving diffeomorphism

$$\rho : \nu_1^c \times \nu_3^c \to \mathcal{W}^c \tag{4.3}$$

between fiber bundles that preserves base points $(z_1, 0)$ and is the identity on the fiber over 0 (that is, ν_3^c). Thus, $\rho(z_1, z_3) \in \mathcal{U}_{z_1}$.

Theorem 4.3. *Using ρ as defined in (4.3), the dynamics on the center manifold $\mathcal{W}^c$ of (4.1) can be written on $\nu_1^c \times \nu_3^c$ and it has the form*

$$\begin{aligned} \dot{z}_1 &= g_1(z_1), \\ \dot{z}_3 &= g_3(z_1, z_3) \end{aligned} \tag{4.4}$$

for some functions g_1 and g_3 and coordinates z_1 on ν_1^c and z_3 on ν_3^c.

Proof. Let Φ_t be the flow of the vector field restricted to $\mathcal{W}^c$. The flow of the pull-back vector field on $\nu_1^c \times \nu_3^c$ is

$$\Psi_t = \rho^{-1} \Phi_t \rho.$$

Since ρ preserves fibers, $\rho(z_1, z_3) = (z_1, \tau(z_1, z_3))$, where (z_1, z_3) are coordinates on $\nu_1^c \times \nu_3^c$ and τ is some function. It follows that ρ^{-1} has the same form since it also preserves fibers.

It follows from Lemma 4.1 and the form of ρ that $\Phi_t \rho$ has the feedforward form

$$\Phi_t(\rho(z_1, z_3)) \equiv \Phi_t(z_1, \tau(z_1, z_3)) = (\phi_{1t}(z_1), \sigma_t(z_1, z_3)) \tag{4.5}$$

for some functions σ_t. Applying ρ^{-1} to (4.5) shows that the first coordinate of Ψ_t depends only on z_1. Hence the system of ODEs on $\mathcal{W}^c$ has the form (4.4) and is feedforward. ∎

5. Codimension-2 mode interactions. In this section, we summarize the main results for codimension-2 bifurcations when the central network contains two critical path components with one downstream of the other (and possibly nodes in between). Throughout this section, we analyze the dynamics of each system using the center manifold network associated with the given central network. Section 4 shows that the center manifold network inherits the feedforward structure of the critical components in the central network. This leads to four possible mode interactions, defined by whether the eigenvalues of each critical component correspond to steady-state or Hopf bifurcation.

The feedforward structure of the center manifold network leads to generic behavior of the mode interactions that is different from generic behavior in the context of general vector fields (which arise in networks with all-to-all coupling).

Remark 5.1. One manifestation of this difference is the existence of a new type of solution in the center manifold network for the four mode interactions. In the steady-state/steady-state and steady-state/Hopf mode interactions, these solutions are invariant sets where the coordinate of the upstream node is constant and the coordinates of the downstream node are not. The flow-invariant set on which these solutions exist can act as a boundary that other trajectories cannot cross, thereby partitioning phase space. ◇

For each of the four mode interactions described in this section, we begin with the center manifold vector field, identify a singularity-theoretic normal form and its universal unfolding, and classify the small amplitude steady-state and periodic solutions as a function of unfolding parameters. We discuss singularity theory in section SM2, which summarizes all the required concepts and results. However, we give brief indications of the key steps as we proceed.

5.1. Steady-state/steady-state mode interaction. In the steady-state/steady-state mode interaction, the Jacobian associated with each critical component of the original network has a single zero eigenvalue, and each critical component corresponds to a one-dimensional phase space on the center manifold. In this case, the vector field on the center manifold has the form

$$\begin{aligned} \dot{x} &= f(x), \\ \dot{y} &= g(x,y), \end{aligned} \tag{5.1}$$

where $x, y \in \mathbb{R}$. We assume that the origin is an equilibrium, so $f(0) = g(0,0) = 0$. The Jacobian of (5.1) has two zero eigenvalues at the origin, so $f_x(0) = g_y(0,0) = 0$.

The goal is to identify a normal form and show that any vector field of the form (5.1), with the associated defining conditions, is equivalent to that normal form, assuming suitable nondegeneracy conditions. We define equivalence in terms of transformations that preserve the center manifold structure, that is, the variable dependence of the functions for each center manifold node. To apply singularity theory, we must define when two bifurcation problems in (5.1) are (strongly) equivalent.

Definition 5.2. *Maps* $F(x,y) = (f(x), g(x,y))$ *and* $\hat{F}(x,y) = (\hat{f}(x), \hat{g}(x,y))$ *are* strongly equivalent *if there exist* $a(x), \phi(x), b(x,y), c(x,y), \psi(x,y)$ *such that*

$$\begin{bmatrix} \hat{f}(x) \\ \hat{g}(x,y) \end{bmatrix} = \begin{bmatrix} a(x) & 0 \\ b(x,y) & c(x,y) \end{bmatrix} \begin{bmatrix} f(\phi(x)) \\ g(\phi(x), \psi(x,y)) \end{bmatrix}, \tag{5.2}$$

where $\phi(0) = \psi(0,0) = 0$ *and* $a(0), c(0,0), \phi_x(0), \psi_y(0,0) > 0$.

In section SM3, we prove the following.

Theorem 5.3. *Assume that* (5.1) *satisfies the defining conditions*

$$f(0) = f_x(0) = g(0,0) = g_y(0,0) = 0 \tag{5.3}$$

and the nondegeneracy conditions

$$g_x(0,0) \neq 0,\ f_{xx}(0) \neq 0,\ g_{yy}(0,0) \neq 0. \tag{5.4}$$

Then $F(x,y) = (f(x), g(x,y))$ is strongly equivalent to the normal form $\hat{F}(x,y)$ given by

$$\begin{aligned} \hat{f}(x) &= \varepsilon_p x^2, \\ \hat{g}(x,y) &= \varepsilon_q x + \varepsilon_t y^2, \end{aligned} \tag{5.5}$$

where

$$\varepsilon_q = \operatorname{sign}(g_x(0,0)),\ \varepsilon_p = \operatorname{sign}(f_{xx}(0)),\ \varepsilon_t = \operatorname{sign}(g_{yy}(0,0)).$$

Theorem 5.3 is useful only if the set of admissible vector fields with a steady-state/steady-state mode interaction that satisfies the mode interaction degeneracy conditions (5.3) includes vector fields that satisfy the nondegeneracy conditions (5.4). In the following, we prove more:

Proposition 5.4. *Consider two path components in a network such that one is downstream of the other and a pair of functions $f : \mathbb{R} \to \mathbb{R}$ and $g : \mathbb{R}^2 \to \mathbb{R}$ such that $f(0) = f'(0) = 0$ and $g(0,0) = g_y(0,0) = 0$. Then there exists an admissible vector field F whose center manifold restriction is given by (5.1), where f is the component of the vector field associated with the upstream path component and g is the component of the vector field associated with the downstream path component.*

Proof. Given two path components with one downstream of the other, there exists a path consisting of $n+1$ distinct nodes that connects a node p_0 in the upstream path component to a node p_n in the downstream path component. We denote the nodes along this path as p_i for $i = 1, \dots, n-1$ and denote the remaining nodes in the network by p_s where $s > n$.

We construct an admissible vector field in the following way. Associate the coordinate $z_j \in \mathbb{R}$ with the node p_j, and define the admissible vector field F by

$$\begin{aligned} \dot{z}_0 &= f(z_0), \\ \dot{z}_i &= -z_i + z_{i-1} + f(z_i), \qquad 1 \le i < n, \\ \dot{z}_n &= g(z_{n-1}, z_n), \\ \dot{z}_s &= -z_s, \qquad\qquad\qquad\quad s > n, \end{aligned} \tag{5.6}$$

for these nodes.

We have assumed that the origin is an equilibrium; that is, $f(0) = 0$ and $g(0,0) = 0$. We have also assumed that the Jacobian of F evaluated at the origin is lower triangular with two zero eigenvalues (that is, $f'(0) = g_{z_n}(0,0) = 0$) and the remaining eigenvalues are equal to -1. The center subspace E^c is spanned by a vector w with single nonzero component $w_n = 1$ and a vector v with nonzero components $v_i = 1$ for $i = 0, \dots, n-1$. The center subspace can be parametrized by coordinates $u^c = xv + yw \in E^c$, where $x, y \in \mathbb{R}$.

By construction, the admissible vector field F leaves the center subspace invariant; hence the center subspace is in fact a center manifold for F. Indeed, the restriction of F to E^c is precisely the vector field (5.1). ∎

Remark 5.5. Proposition 5.4 implies that generically admissible vector fields that satisfy the degeneracy conditions (5.3) also satisfy the nondegeneracy conditions (5.4).

Universal unfoldings classify perturbations up to equivalence. Recall that when computing universal unfoldings, we relax the restrictions in Definition 5.2 that $\phi(0)$ and $\psi(0,0)$ vanish.

Theorem 5.6. *The normal form* (5.5) *has codimension-*2*, and a universal unfolding is*

$$\begin{aligned} f(x,\lambda) &= \lambda + \varepsilon_p x^2, \\ g(x,y,\mu) &= \mu + \varepsilon_q x + \varepsilon_t y^2. \end{aligned} \tag{5.7}$$

Remark 5.7.

(a) Since the Jacobian is always lower triangular, Hopf bifurcation cannot occur in the universal unfolding (5.7). This contrasts with the codimension-2 Takens–Bogdanov singularity (a steady-state/steady-state mode interaction), where we expect both periodic solutions and homoclinic orbits to occur (Guckenheimer and Holmes (1983)). Neither of these solution types appears in (5.7).

(b) On the other hand, solutions of the type described in Remark 5.1 exist in the universal unfolding (5.7). These solutions are invariant lines where $x(t)$ is constant and $y(t)$ is not. They appear in pairs where one is stable in the x-direction and the other is unstable in that direction. These pairs of solutions are "heteroclinic-like" in that solutions with initial conditions between the two invariant lines converge to one line in forward time and to the other line in backward time.

To state the next result, we must briefly discuss the concept of a transition variety. Given a k-parameter family of ODEs parametrized by $\lambda = (\lambda_1, \ldots, \lambda_k) \in \mathbb{R}^k$, generically the set of equilibria or periodic states has the same topology throughout a neighborhood of a point λ_0. Bifurcations occur when this statement is false. It is often possible to classify the relevant points λ_0 according to the type of bifurcation that occurs. For each type of bifurcation, the relevant points λ_0 form the corresponding *transition variety* or *bifurcation set*. See section III.5 of Golubitsky and Schaeffer (1985) in the similar context of qualitative changes to bifurcation diagrams.

We now compute the steady-state solutions as a function of the parameters μ and λ. Changing $\varepsilon_p, \varepsilon_q, \varepsilon_t$ to $-\varepsilon_p, -\varepsilon_q, -\varepsilon_t$ rotates the transition variety in the $\mu\lambda$-plane by 180° and changes the stability of each steady state in both the x- and y-directions. Hence we can assume $\varepsilon_p = -1$ and consider the four cases $\varepsilon_q = \pm 1$, $\varepsilon_t = \pm 1$.

Case 1*:* $\varepsilon_p = \varepsilon_q = \varepsilon_t = -1$. The saddle-node part of the transition variety in parameter space occurs when the Jacobian matrix

$$J = \begin{bmatrix} -2x & 0 \\ -1 & -2y \end{bmatrix}$$

at an equilibrium has a zero eigenvalue. The first case is $x = 0$, which leads to the half line $\lambda = 0$, $\mu \geq 0$. The second case $y = 0$ leads to the parabola $\lambda = \mu^2$; see Figure 12 (left). Each component of the transition variety corresponds to a saddle-node bifurcation.

There are no steady states for $\lambda < 0$; two steady states inside the parabola; and four steady states for parameters in the region between the parabola and the half line. These steady states and their stabilities are listed in Table 3.

The transition varieties here are the boundaries between the four regions. The transitions across these boundaries are conveniently illustrated by the *circulant (or gyrant) bifurcation diagram* of Figure 12 (right). To obtain this diagram, we start in region $\mathbf{I}_+$ ($\lambda < 0$) and plot

Table 3

Steady-state/steady-state mode interaction: Case 1. List of solutions (column 3) and their stabilities (column 4) in each of the regions (column 1) in Figure 12 (left). The entries in I_- *column 3 list the invariant lines.*

	Region	Solutions (x, y)	Eigenvalues
I_-	$0 < \lambda < \mu^2$	$(\sqrt{\lambda}, y)$	$-*$
	$\mu < 0;\ y \in \mathbb{R}$	$(-\sqrt{\lambda}, y)$	$+*$
II	$0 < \lambda < \mu^2$	$\left(\sqrt{\lambda}, +\sqrt{\mu - \sqrt{\lambda}}\right)$	$--$
	$0 < \mu$	$\left(\sqrt{\lambda}, -\sqrt{\mu - \sqrt{\lambda}}\right)$	$-+$
		$\left(-\sqrt{\lambda}, +\sqrt{\mu + \sqrt{\lambda}}\right)$	$+-$
		$\left(-\sqrt{\lambda}, -\sqrt{\mu + \sqrt{\lambda}}\right)$	$++$
III	$\mu^2 < \lambda$	$\left(-\sqrt{\lambda}, +\sqrt{\mu + \sqrt{\lambda}}\right)$	$+-$
		$\left(-\sqrt{\lambda}, -\sqrt{\mu + \sqrt{\lambda}}\right)$	$++$

the equilibria, following a counterclockwise circle around the origin in the $\mu\lambda$-plane. It is also helpful to track x-invariant sets defined by $f(x) = 0$, in addition to the steady states.

In region I_+, there are no steady states or x-invariant sets in the phase space. Moving from region I_+ to region II across the transition line $\mathrm{SN_d}$, two pairs of steady states appear, each pair appearing simultaneously through a saddle-node bifurcation. This transition results in four steady-state solutions, Table 3 column 3. The set of four equilibria is invariant under reflection $y \to -y$.

Moving from region II to region III across the transition line SN_+ results in the loss of the two equilibria with $x > 0$ through a saddle-node bifurcation. At the transition curve SN_+, there are three steady-state solutions. In region III, only the two steady states remain; however, an x-invariant line defined by $x = \sqrt{-\lambda}$ persists as a remnant of the pair of steady states from region II that have been lost.

The remaining pair of steady-state solutions in region III disappears through a saddle-node bifurcation when crossing the transition curve SN_-. Along SN_- both a single equilibrium at $(-\sqrt{\lambda}, 0)$ and an x-invariant line given by $x = \sqrt{\lambda}$ exist. In I_-, no steady states exist. However, in this region two x-invariant lines given by $x = \pm\sqrt{\lambda}$ partition the phase space into three regions. Finally, as λ decreases through 0, the two x-invariant lines disappear through a saddle-node of $f(x)$ (not a saddle-node of the entire system).

Case 2: $\varepsilon_p = -1$, $\varepsilon_q = \varepsilon_t = -1$. Reversing the signs of ε_q and ε_t maps $\mu \to -\mu$ in the bifurcation diagram, that is, reflects the 2-parameter bifurcation diagram in Figure 12 about the λ-axis. The set of equilibria is preserved under the transformation $\varepsilon_q \to -\varepsilon_q$, $\varepsilon_t \to -\varepsilon_t$, and $\mu \to -\mu$, but the stability of these fixed points changes in the y-direction while remaining the same in the x-direction.

Case 3: $\varepsilon_p = -1$, $\varepsilon_q = 1$, $\varepsilon_t = -1$. $\varepsilon_q \to -\varepsilon_q$ does not affect the bifurcation structure in the $\mu\lambda$-plane or the stability of any equilibrium.

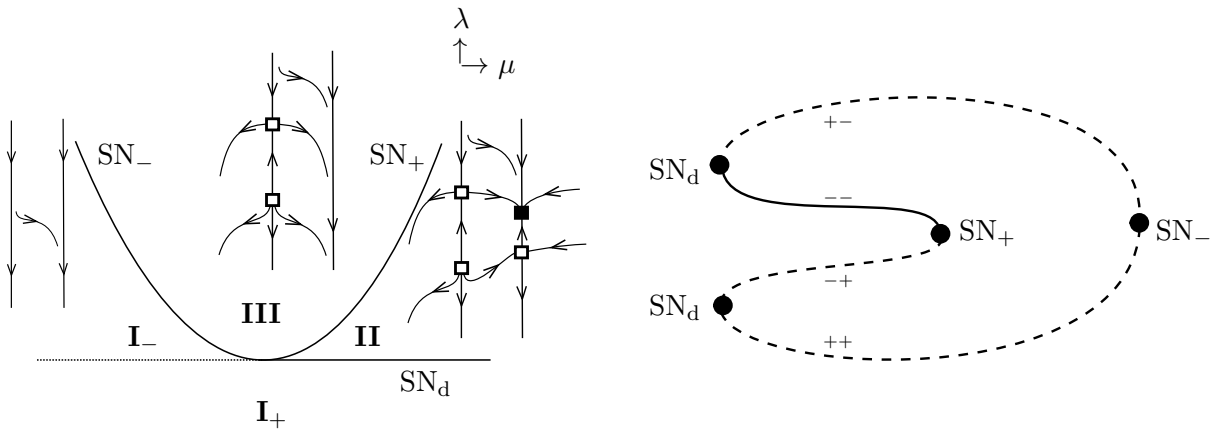

Figure 12. *Steady-state/steady-state mode interactions. Case* 1: $\varepsilon_p = \varepsilon_q = \varepsilon_t = -1$. Left*: Transition variety in the $\mu\lambda$ parameter plane, with phase portraits in the xy phase plane in each connected region of parameter space. Solid curves* $\mathrm{SN_d}$, $\mathrm{SN_+}$, *and* $\mathrm{SN_-}$ *represent a double saddle-node and two single saddle-node transition curves for* (5.7)*. The straight vertical lines in the phase portraits indicate the existence of invariant lines defined by $f(x) = 0$. The dotted half line indicates a saddle-node of invariant lines.* Right*: Circulant bifurcation diagram as a small circle is traversed counterclockwise around the origin in the $\mu\lambda$-plane. The plus and minus signs show the stability of each branch in the x- and y-directions.*

Case 4: $\varepsilon_p = -1$, $\varepsilon_q = -1$, $\varepsilon_t = 1$. $\varepsilon_t \to -\varepsilon_t$ corresponds to transforming $\mu \to -\mu$ in the bifurcation diagram.

5.2. Hopf/steady-state mode interaction. In a Hopf/steady-state mode interaction, the Jacobian associated with the critical component where the Hopf bifurcation occurs has a pair of purely imaginary eigenvalues, whereas the Jacobian associated with the other component has a single zero eigenvalue. On the center manifold, the component associated with the Hopf bifurcation has a two-dimensional phase space. In this case, the center manifold vector field has the form

$$\begin{aligned} \dot{X} &= f(X), \\ \dot{y} &= g(X, y), \end{aligned} \tag{5.8}$$

where $X \in \mathbb{R}^2$ and $y \in \mathbb{R}$. Assume that the origin is an equilibrium so that $f(0) = g(0,0) = 0$. At the origin, the Jacobian of (5.8) has a pair of purely imaginary eigenvalues and a zero eigenvalue, so that $\mathrm{D}f(0)$ has eigenvalues $\pm i$ and $g_y(0,0) = 0$. We show in section SM4 that under these assumptions, Lyapunov–Schmidt reduction leads to a two-dimensional map F with $\mathbf{Z}_2$-symmetry $\sigma(x,y) = (-x,y)$. We obtain the following.

Theorem 5.8. *Assume* (5.8) *satisfies the defining conditions $f(0) = g(0,0) = 0$, $Df(0)$ has eigenvalues $\pm i$, and $g_y(0,0) = 0$. Then there exists a smooth map*

$$F(x,y) = \begin{bmatrix} r(u)x \\ g(u,y) \end{bmatrix}, \quad u = x^2, \tag{5.9}$$

where $r(0) = 0$ and $g(0,0) = 0$, such that locally, solutions to $F(x,y) = 0$ with $x \geq 0$ are in one-to-one correspondence with small amplitude periodic solutions to (5.8) with period near 2π.

Theorem 5.8 reduces finding periodic solutions of (5.8) to finding the zeros of a two-dimensional system (5.9) with $\mathbf{Z}_2$-symmetry. The goal is then to identify a normal form and to show that all vector fields of the form (5.9) satisfying the associated defining and nondegeneracy conditions are equivalent. For this, we need a $\mathbf{Z}_2$-symmetric version of Definition 5.2.

Definition 5.9. *A map $F(x,y) = (r(u)x, g(u,y))$ and $G(x,y)$ are strongly $\mathbf{Z}_2$-equivalent if*

$$G(x,y) = \begin{bmatrix} a(u) & 0 \\ b(u,y)x & c(u,y) \end{bmatrix} \begin{bmatrix} r(\phi(u)^2 u)\phi(u)x \\ g(\phi(u)^2 u, \psi(u,y)) \end{bmatrix}, \tag{5.10}$$

where $\psi(0,0) = 0$ and $a(0)$, $c(0,0)$, $\phi(0)$, $\psi_y(0,0) > 0$.

Remark 5.10. The difference between equivalence in Definition 5.2 and $\mathbf{Z}_2$-equivalence in Definition 5.9 is that the change of coordinates is $\mathbf{Z}_2$-equivariant. That is, $\gamma G(x,y) = G(\gamma(x,y))$, where $\gamma(x,y) = (-x,y)$. This leads to the form (5.10) for strong $\mathbf{Z}_2$-equivalence. Requirements on ϕ, ψ, a, and c follow from the restrictions in Definition 5.2.

Theorem 5.11. *Assume that (5.9) satisfies the defining conditions*

$$r(0) = g(0,0) = g_y(0,0) = 0 \tag{5.11}$$

and the nondegeneracy conditions

$$r_u(0) \neq 0, \quad g_u(0,0) \neq 0, \quad g_{yy}(0,0) \neq 0. \tag{5.12}$$

Then $F(x,y) = (r(u)x, g(u,y))$ is strongly $\mathbf{Z}_2$-equivalent to the normal form $\hat{F}$ given by

$$\begin{aligned} \hat{r}(u)x &= \varepsilon_p u x, \\ \hat{g}(u,y) &= \varepsilon_q u + \varepsilon_t y^2, \end{aligned} \tag{5.13}$$

where

$$\varepsilon_p = \operatorname{sign}(r_u(0)), \quad \varepsilon_q = \operatorname{sign}(g_u(0,0)), \quad \varepsilon_t = \operatorname{sign}(g_{yy}(0,0)).$$

Theorem 5.11 is useful only if Hopf/steady-state mode interaction admissible vector fields satisfying the mode interaction defining conditions (5.11) are rich enough to satisfy the nondegeneracy conditions (5.12). We would like to prove a result analogous to the steady-state/steady-state Proposition 5.4 for the Hopf/steady-state mode interaction. At the very least, we would like to exhibit one example of an admissible vector field for a given network that satisfies both the defining conditions (5.11) and the nondegeneracy conditions (5.12). If we can do so, the desired result can be obtained by arguments based on algebraic geometry. What we do know so far is that, given any network, we can construct an admissible vector field that satisfies the defining conditions by considering a subnetwork consisting of a directed ring with a feedforward chain coming off of one of the nodes. Similar statements hold for the remaining codimension-2 mode interactions.

Because the critical path component associated with the steady-state bifurcation (zero eigenvalue) is downstream from the one associated with the Hopf bifurcation (complex conjugate pair of pure imaginary eigenvalues), there exists a path from a node h in the upstream critical component to a node s in the downstream critical component. Moreover, because the upstream component is associated with Hopf bifurcation, it contains at least two nodes. We can therefore construct a path connecting node h to another node in the upstream critical component going in both directions. A directed ring exists within this bidirectional path and can be found by clipping sections of the path beyond nodes that are contained along both the path to and from h. Any admissible vector field on this ring-and-chain subnetwork along with dynamics on other nodes o defined by $\dot{x}_o = -x_o$ will be admissible on the full network.

To classify perturbations up to equivalence, we use universal unfoldings. Again, we relax the restrictions in Definition 5.9 that $\psi(0,0)$ vanishes to compute universal unfoldings.

Theorem 5.12. *The normal form* (5.13) *has codimension-*2*. A universal unfolding is*

$$\begin{aligned} r(u,\lambda)x &= (\lambda + \varepsilon_p u)x, \\ g(x,y,\mu) &= \mu + \varepsilon_q u + \varepsilon_t y^2. \end{aligned} \tag{5.14}$$

Remark 5.13. In Hopf/steady-state mode interaction, the x-invariant solutions described in Remark 5.1 appear in the universal unfolding (5.14). The invariant line with $x > 0$ on the Lyapunov–Schmidt reduced space corresponds to a flow-invariant solid cylinder aligned along the y-axis in the center manifold phase space. When present, this invariant set partitions phase space, and "heteroclinic-like" orbits appear that connect the flow-invariant line at the center of the cylinder $x = 0$ with the boundary of the solid cylinder; see region I_+ in Figure 13 (right). In one direction, these trajectories approach helical oscillation on the boundary of the cylinder, and in the other they approach the central line of the cylinder.

It is now straightforward to compute the steady-state solutions of (5.14) as a function of the parameters μ and λ. Locally these equilibria are in one-to-one correspondence with periodic solutions of (5.8) by Theorem 5.8. We are interested only in nonnegative solutions for the variable x, which relate to the amplitude of periodic orbits of (5.8). As in section 5.1, it is sufficient to assume $\varepsilon_p = -1$ and consider the four cases $\varepsilon_t = \pm 1$, $\varepsilon_q = \pm 1$.

Case 1*:* $\varepsilon_p = \varepsilon_q = \varepsilon_t = -1$. The bifurcation in the $\mu\lambda$ parameter space occurs when the Jacobian

$$J = \begin{bmatrix} \lambda - 3x^2 & 0 \\ -2x & -2y \end{bmatrix}$$

at an equilibrium has a zero eigenvalue. The first case is $\lambda - 3x^2 = 0$, which leads to the half line $\lambda = 0$, $\mu \geq 0$ corresponding to a pitchfork bifurcation (Hopf bifurcation in the full three-dimensional system (5.8)). The second case $y = 0$ leads to two saddle-node bifurcations given by $\mu = 0$ and the half line $\mu - \lambda = 0$, $\lambda \geq 0$, where the former corresponds to a saddle-node of steady states in (5.8) and the latter to a saddle-node bifurcation of periodic orbits (SNPO) in (5.8). See Figure 13 (left).

There are no steady states for $\mu < 0$; two steady states for $\lambda < 0$, $\mu > 0$, and $\lambda > \mu > 0$; and four steady states for $\mu > \lambda > 0$. Unlike the steady-state/steady-state mode interaction, x-invariant lines do not always appear in pairs; in fact, one x-invariant line given by $x = 0$

persists throughout the full parameter space. These steady states, x-invariant solutions, and their stabilities are listed in Table 4.

Table 4

List of solutions (column 3) and their stabilities (column 4) in each of the regions (column 1) in Figure 13 (left). The entries in I_+ *and* I_- *column 3 list the invariant lines.*

	Region	Solutions (x, y)	Eigenvalues
II	$\lambda < 0$ $0 < \mu$	$(0, +\sqrt{\mu})$ $(0, -\sqrt{\mu})$	$--$ $-+$
III	$0 < \lambda$ $\lambda < \mu$	$(0, +\sqrt{\mu})$ $(0, -\sqrt{\mu})$ $\left(\sqrt{\lambda}, +\sqrt{\mu - \lambda}\right)$ $\left(\sqrt{\lambda}, -\sqrt{\mu - \lambda}\right)$	$+-$ $++$ $--$ $-+$
IV	$\mu < \lambda$ $0 < \mu$	$(0, +\sqrt{\mu})$ $(0, -\sqrt{\mu})$	$-+$ $++$
I_+	$0 < \lambda$ $\mu < 0$	$(0, *)$ $\left(\sqrt{\lambda}, *\right)$	$+*$ $-*$
I_-	$\lambda < 0$ $\mu < 0$	$(0, *)$	$-*$

The circulant diagram in Figure 13 (right) shows transitions across the boundaries between the five regions. Begin in region I_-: there are no steady states, but there is one x-invariant line $x = 0$, which partitions the phase space into two regions. Moving from region I_- to region II across the transition line SN_- (with $\lambda < 0$), the first pair of steady states, Table 4 column 3, appears through a saddle-node bifurcation. At the transition line SN_-, there is one steady-state solution $(x, y) = (0, 0)$.

Moving from region II to region III across the transition line $\mathrm{H_d}$ (with $\mu > 0$), each of the two steady states that appeared at $\mu = 0$ splits into three steady states through a pair of pitchfork bifurcations. This creates six steady states. Four have nonnegative x values; see Table 4 column 3 and Figure 13 (left). The two steady states with positive x correspond to the two periodic solutions of (5.8) born at Hopf bifurcations.

Moving from region III to region IV across the transition line SNPO results in the loss of the equilibria with $x \neq 0$ through a saddle-node bifurcation. At the transition curve SNPO, there are three steady-state solutions $(0, 0)$, $(0, \pm\sqrt{\mu})$. Only the two equilibria at $(0, \pm\sqrt{\mu})$ remain in region IV; these disappear through a saddle-node bifurcation when crossing the transition curve SN_+. Along SN_+ there is one steady-state solution at $(0, 0)$. In region I_+, no steady states exist. However, in this region there are two x-invariant lines $x = 0$ (unstable in the x-direction) and $x = \sqrt{\lambda}$ (stable in the x-direction). These two solutions are "heteroclinic-like" as discussed in section 5.1, and they partition the two-dimensional phase space into three regions. Finally, as λ decreases through 0, the x-invariant line given by $x = \sqrt{\lambda}$ disappears through a pitchfork bifurcation of $f(x)$ (not a pitchfork in the entire system) and only $x = 0$ persists.

Case 2: $\varepsilon_p = -1$, $\varepsilon_q = +1$, $\varepsilon_t = -1$. Reversing the sign of ε_q changes the SNPO transition line to $\lambda + \mu = 0$, $\lambda \geq 0$, which is to the left of the line SN_+. In contrast to Case 1, the two periodic solutions of (5.8) that appeared at the transition line $\mathrm{H_d}$ persist after the two steady

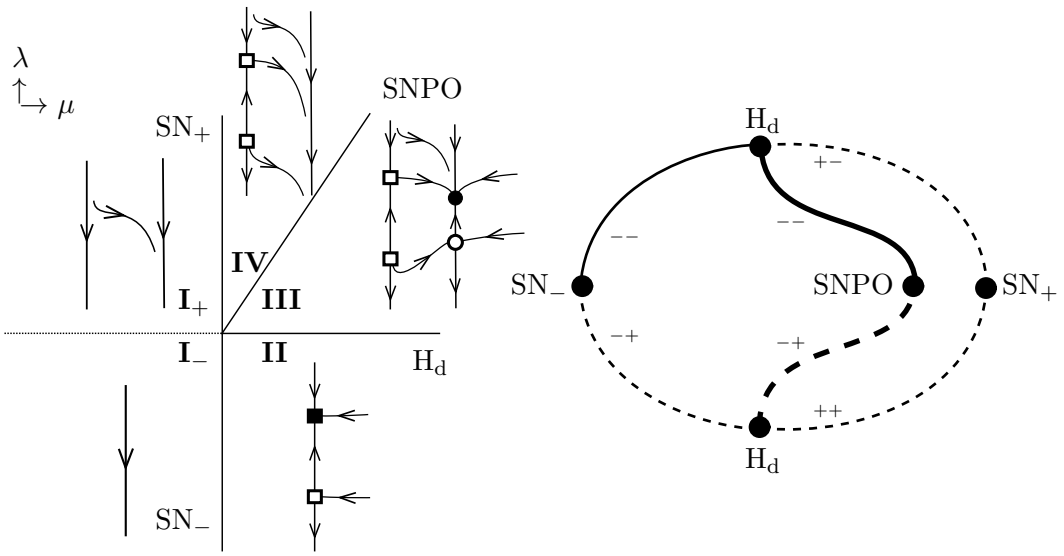

Figure 13. *Hopf/steady-state mode interaction. Case* 1*:* $\varepsilon_p = \varepsilon_q = \varepsilon_t = -1$. Left*: Transition variety in the* $\mu\lambda$ *parameter plane, with phase portraits in the* xy *phase plane in each connected region of parameter space. Solid curves* SN_-, SN_+, SNPO*, and* $\mathrm{H_d}$ *represent three saddle-node curves and a double pitchfork transition curve for* (5.14) *and correspond to two saddle-nodes, a saddle-node of periodic orbits, and a double Hopf bifurcation for* (5.8)*. In the phase portraits, the square and circle symbols correspond to the steady states and the periodic solutions of the full three-dimensional system* (5.8)*, while the straight vertical lines indicate* x*-invariant lines defined by* $f(x) = 0$. Right*: Circulant bifurcation diagram as a small circle is traversed counterclockwise around the origin in the* $\mu\lambda$*-plane. The plus and minus signs show the stability of each branch in the* x*- and* y*-directions. Thicker lines indicate the periodic solutions of* (5.8)*. The dotted half line in the left-hand figure indicates a "pitchfork" of the invariant line* $x = 0$ *to the invariant lines* $x = 0$ *and* $x = \sqrt{\lambda}$ *as* λ *increases through* 0.

states disappear at SN_+, going counterclockwise in a circle around the origin in the $\mu\lambda$-plane. Changing $\varepsilon_q \to -\varepsilon_q$ does not affect the stability of any equilibria. See Figure 14.

Case 3: $\varepsilon_p = -1$, $\varepsilon_q = +1$, $\varepsilon_t = +1$. Reversing the sign of ε_q and ε_t (from Case 1) is equivalent to a transformation $\lambda \to -\lambda$ and a change of stability in the y-direction.

Case 4: $\varepsilon_p = -1$, $\varepsilon_q = -1$, $\varepsilon_t = +1$. Reversing the sign of ε_q and ε_t (from Case 2) is equivalent to a transformation of $\lambda \to -\lambda$ and a change of stability in the y-direction.

5.3. Steady-state/Hopf mode interaction. Assume, as in the previous two subsections, that there are two critical components with one downstream of the other. The steady-state/Hopf mode interaction differs from the Hopf/steady-state mode interaction: the Jacobian associated with the upstream critical component of the original network has a single zero eigenvalue, whereas the Jacobian associated with the downstream critical component has a complex conjugate pair of pure imaginary eigenvalues. The vector field on the center manifold has the form

$$\begin{aligned} \dot{x} &= f(x), \\ \dot{Y} &= g(x, Y), \end{aligned} \tag{5.15}$$

where $x \in \mathbb{R}$, $Y \in \mathbb{R}^2$, $f(0) = 0$, and $g(0, 0) = 0$.

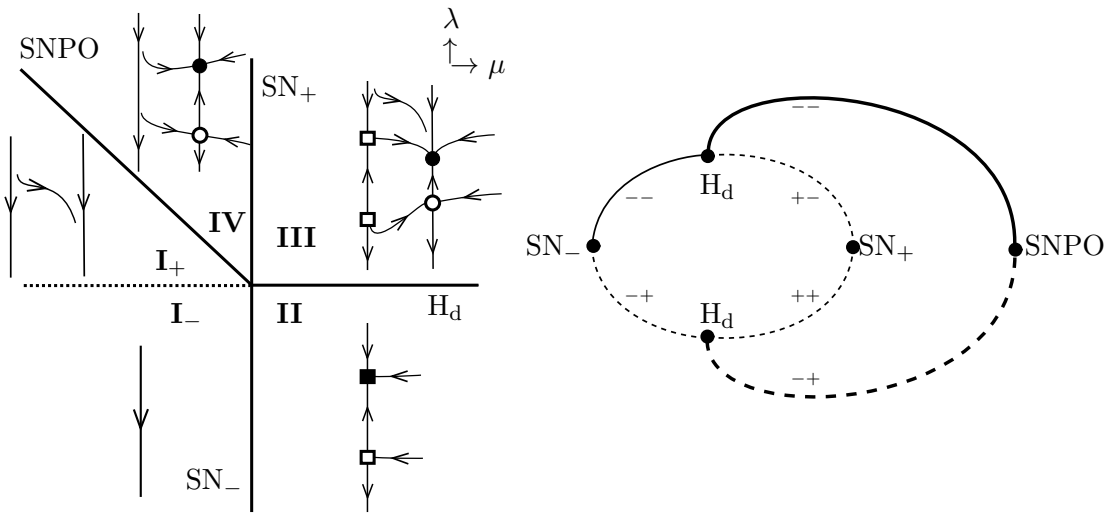

Figure 14. *Hopf/steady-state mode interaction. Case* 2*: Labels and symbol codings have the same meanings as in Figure* 13. Left: *Transition varieties in the $\mu\lambda$ parameter plane and phase portraits in the xy phase plane for the regions they determine.* Right*: Circulant bifurcation diagram.*

At the origin, the Jacobian of (5.15) has a zero eigenvalue and a pair of purely imaginary eigenvalues, namely

$$f_x(0) = 0, \qquad \operatorname{tr} \mathrm{D}_Y g(0,0) = 0, \qquad \det \mathrm{D}_Y g(0,0) > 0.$$

Rescaling time, we can assume $\det \mathrm{D}_Y g(0,0) = 1$ and the eigenvalues are $\pm i$.

Section SM4 employs Lyapunov–Schmidt reduction to reduce finding steady states and periodic orbits of (5.15) to finding zeros of a map associated with two one-dimensional nodes. The goal is to identify a normal form for the reduced map (5.16) below, using equivalences that preserve the network structure of the center manifold.

Theorem 5.14. *Assume that* (5.15) *has an equilibrium at the origin that undergoes a steady-state/Hopf mode interaction. The defining conditions are*

$$f(0) = 0, \qquad g(0,0) = 0, \qquad f_x(0) = 0, \qquad \operatorname{tr} \mathrm{D}_Y g(0,0) = 0, \qquad \det \mathrm{D}_Y g(0,0) = 1.$$

Then there exists a smooth map on $\mathbb{R} \times \mathbb{R}$ of the form

$$F(x,y) = (f(x), r(x,v)y), \tag{5.16}$$

where $v = y^2$ and $r(0,0) = 0$, such that locally solutions to $F(x,y) = 0$ with $y \geq 0$ are in one-to-one correspondence with small amplitude periodic solutions to (5.15) *with period near 2π.*

On the reduced system (5.16), the transformations that define equivalence must respect $\mathbf{Z}_2$-symmetry in addition to the network structure of the center manifold.

Definition 5.15. *Maps* $F(x,y) = (f(x), r(x,v)y)$ *and* $\hat{F}(x,y) = (\hat{f}(x), \hat{r}(x,v)y)$ *are strongly* $\mathbf{Z}_2$*-equivalent if there exist* $a(x)$, $\phi(x)$, $b(x,v)$, $c(x,v)$, $\phi(x,v)$ *such that*

$$\hat{F}(x,v) = \begin{bmatrix} a(x) & 0 \\ b(x,v)y & c(x,v) \end{bmatrix} \begin{bmatrix} f(\phi(x)) \\ r(\phi(x), \psi(x,v)y) \end{bmatrix}, \tag{5.17}$$

where $v = y^2$, $\phi(0) = 0$, *and* $a(0)$, $c(0,0)$, $\phi_x(0)$, $\psi(0,0) > 0$.

Remark 5.16. This differs from equivalence as in Definition 5.9 because it requires equivariance under a different representation of $\mathbf{Z}_2$, namely $\gamma G(x,y) = G(\gamma(x,y))$, where $\gamma(x,y) = (x,-y)$.

We now state the normal form in terms of the Lyapunov–Schmidt reduced system (5.16), where the variable y represents the amplitude of the periodic orbit in the Y coordinates of (5.15) on the center manifold.

Theorem 5.17. *Assume* (5.16) *satisfies the defining conditions*

$$f(0) = f_x(0) = r(0,0) = 0$$

and the nondegeneracy conditions

$$f_{xx}(0) \neq 0, \quad r_v(0,0) \neq 0, \quad r_x(0,0) \neq 0.$$

Then $F(x,y) = (f(x), r(x,v)y)$, *where* $v = y^2$, *is strongly* $\mathbf{Z}_2$*-equivalent, as defined in* (5.15), *to the normal form* $\hat{F}(x,y) = (\hat{f}(x), \hat{r}(x,v)y)$ *given by*

$$\begin{aligned} \hat{f}(x) &= \varepsilon_p x^2, \\ \hat{r}(x,v)y &= (\varepsilon_t v + \varepsilon_s x)\, y, \end{aligned} \tag{5.18}$$

where

$$\varepsilon_p = \operatorname{sign}(f_{xx}(0)), \quad \varepsilon_t = \operatorname{sign}(r_v(0,0)), \quad \varepsilon_s = \operatorname{sign}(r_x(0,0)).$$

We note that remarks on genericity that are similar to those made after Theorem 5.11 also hold for this codimension-2 bifurcation.

As usual, we compute a universal unfolding by relaxing the restriction in Definition 5.15 that $\phi(0)$ vanishes.

Theorem 5.18. *The normal form* (5.18) *has codimension-*2*. A universal unfolding is*

$$\begin{aligned} f(x) &= \lambda + \varepsilon_p x^2, \\ r(x,v)y &= (\mu + \varepsilon_s x + \varepsilon_t v)\, y. \end{aligned} \tag{5.19}$$

Remark 5.19. Both the steady-state/Hopf mode interaction (5.19) and the Hopf/steady-state mode interaction (5.14) are very different from what is observed for the analogous mode interaction in general vector fields. In particular, 2-tori, which are observed in general vector fields, are not possible because of the feedforward structure of the network.

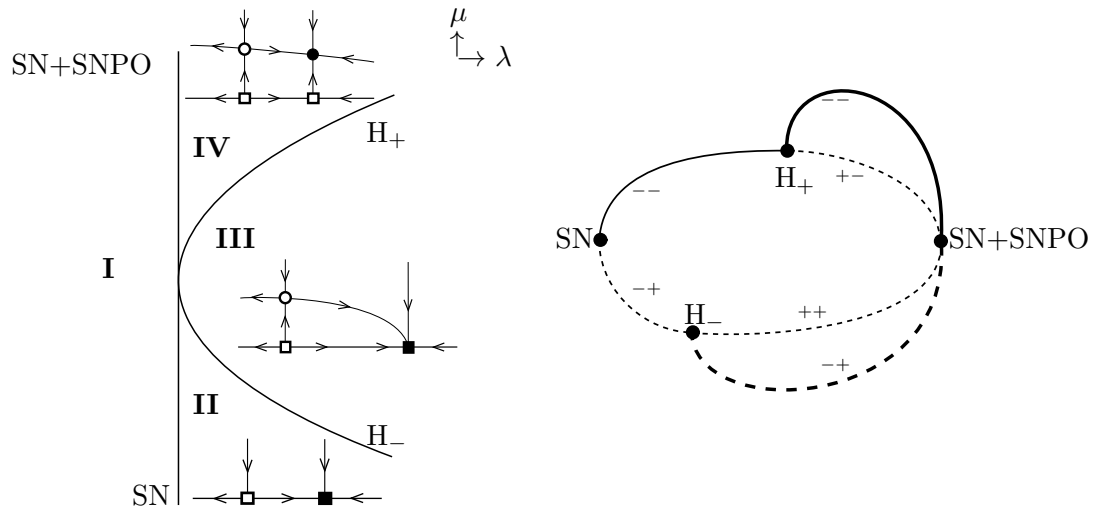

Figure 15. *Steady-state/Hopf mode interaction. Case* 1*:* $\varepsilon_p = -1$, $\varepsilon_s = -1$, $\varepsilon_q = -1$. Left*: Transition variety in the* $\lambda\mu$*-plane, with phase portraits in the* xy *phase plane in each connected region of parameter space. Solid curves* SN, SN + SNPO, H_+, *and* H_- *represent saddle-node, double saddle-node, and pitchfork transition curves for* (5.19). *They correspond to saddle-node, saddle-node and saddle-node of periodic orbits, and Hopf bifurcation curves for* (5.15). Right*: Circulant bifurcation diagram. Plus and minus signs show the stability of each branch in the* x*- and* y*-directions. Thicker lines indicate the periodic solutions of* (5.8).

Remark 5.20. In steady-state/Hopf mode interaction, the x-invariant solutions described in Remark 5.1 exist in the universal unfolding (5.19). These invariant lines on the Lyapunov–Schmidt reduced space correspond to the flow-invariant planes perpendicular to the x-axis in the center manifold phase space. Similar to the steady-state/steady-state mode interaction, they appear in pairs where one is stable in the x-direction and the other is unstable in that direction. When present, the invariant sets partition phase space, and "heteroclinic-like" orbits appear that connect the two flow-invariant planes. In one direction, these trajectories approach one plane, and in the other they approach the other plane.

We discuss all possible cases described by (5.19) in terms of the signs of the coefficients as follows. We fix $\varepsilon_p = -1$ and consider the four cases with $\varepsilon_s = \pm 1$ and $\varepsilon_t = \pm 1$. The remaining four possibilities are obtained from these by noting that flipping the sign of all three coefficients is equivalent to changing the sign of the parameters μ and λ, and changing the stability of each equilibrium in both the x- and the y-directions. We provide a detailed discussion when $\varepsilon_p = \varepsilon_s = \varepsilon_t = -1$ (Table 5, Figure 15) and present the other three cases in terms of the signs of coefficients ε_s and ε_t.

Case 1*:* $\varepsilon_p = -1$, $\varepsilon_s = -1$, $\varepsilon_t = -1$. The Jacobian of (5.19) linearized about an equilibrium (x, y) is

$$J = \begin{bmatrix} -2x & 0 \\ -y & \mu - 3y^2 - x \end{bmatrix}.$$

Table 5

Steady-state/Hopf mode interaction. Case 1*: List of steady-state equilibria (SS), periodic orbits (PO), and flow-invariant sets (FIS) with* $y \geq 0$*. The region in parameter space where each exists is given in column* 1 *in terms of the four regions identified in Figure* 15 *(left) and in terms of parameter regimes in column* 2*. The coordinates and type are given in columns* 3 *and* 4*, respectively, and the stabilities of the equilibria are in column* 5*.*

	Region	Solutions (x, y)	Type	Eigenvalues
I-IV		$(*, 0)$	FIS	
II-IV	$0 < \lambda$	$\left(+\sqrt{\lambda}, *\right)$	FIS	$-*$
		$\left(-\sqrt{\lambda}, *\right)$	FIS	$+*$
II	$0 < \lambda$	$\left(+\sqrt{\lambda}, 0\right)$	SS	$--$
	$\mu < -\sqrt{\lambda}$	$\left(-\sqrt{\lambda}, 0\right)$	SS	$+-$
III	$\mu^2 < \lambda$	$\left(+\sqrt{\lambda}, 0\right)$	SS	$--$
		$\left(-\sqrt{\lambda}, 0\right)$	SS	$++$
		$\left(-\sqrt{\lambda}, \sqrt{\mu + \sqrt{\lambda}}\right)$	PO	$+-$
IV	$0 < \lambda$	$\left(+\sqrt{\lambda}, 0\right)$	SS	$-+$
		$\left(+\sqrt{\lambda}, \sqrt{\mu - \sqrt{\lambda}}\right)$	PO	$--$
	$\sqrt{\lambda} < \mu$	$\left(-\sqrt{\lambda}, 0\right)$	SS	$++$
		$\left(-\sqrt{\lambda}, \sqrt{\mu + \sqrt{\lambda}}\right)$	PO	$+-$

The eigenvalues can be read off directly as $-2x$ and $\mu - 3y^2 - x$. For all parameter values, the line $y = 0$ is flow-invariant in the two-dimensional Lyapunov–Schmidt reduced space. In the three-dimensional center manifold, this line corresponds to the line $(x, 0, 0)$ (see (5.15)). When $\lambda > 0$, a pair of equilibria $(x, y) = (\pm\sqrt{\lambda}, 0)$ exist; they are created at a saddle-node bifurcation along this y-invariant line at $\lambda = 0$. Each of these two equilibria exists as part of an x-invariant line in the two-dimensional space that corresponds to an x-invariant plane in the three-dimensional center manifold. If additionally $\mu > 0$, there is a saddle-node of periodic orbits bifurcating simultaneously at $\lambda = 0$. These periodic orbits correspond to the pair of steady-state equilibria

$$(x, y) = \left(\pm\sqrt{\lambda}, \sqrt{\mu \mp \sqrt{\lambda}}\right)$$

in the two-dimensional space. Each of the two periodic orbits created through this bifurcation exists within the x-invariant plane containing the equilibrium point with the same x-coordinate. The curve $\lambda = \mu^2$ defines two families of Hopf bifurcations, each connecting the steady state $y = 0$ to the periodic orbit with the same x-coordinate. Figure 15 (left) shows these transition varieties in the (λ, μ)-plane, along with representative phase portraits within each connected region of the complement.

The circulant diagram of Figure 15 (right) shows transitions across the boundaries between the four regions in the $\lambda\mu$-plane. The dynamics along the x-direction is y-invariant, and the line $y = 0$ (corresponding to the line $Y = 0$ in the three-dimensional center manifold) is flow-invariant and persists for all parameter values. In region I, there are no equilibria since

$\lambda < 0$; trajectories approach $-\infty$ along the x-direction. A saddle-node bifurcation occurs as we cross from region I into region II, where a stable and an unstable steady-state equilibrium exist on the invariant line $y = 0$. A heteroclinic trajectory along $y = 0$ connects the unstable steady state to the stable steady state. Because the flow along the x-direction is y-invariant, a pair of x-invariant lines (corresponding to flow-invariant planes in the center manifold) is also created along with the equilibria. Each x-invariant subspace contains one of the steady states, and the unstable steady state is in fact stable when restricted to its x-invariant subspace. Moreover, these x-invariant subspaces partition the phase space so that trajectories between them remain trapped for all time. In contrast to the previous two mode interactions, the x-invariant subspaces never exist independently of equilibria. This can be traced back to the persistence of the y-invariant subspace defined by $y = 0$ for all parameter values.

Going from region II to region III, a pitchfork bifurcation of the unstable steady state occurs. This corresponds to a Hopf bifurcation in the center manifold and creates an unstable periodic orbit contained in the x-invariant plane of the unstable steady state. The orbit is unstable to perturbations along the x-direction but stable within the flow-invariant plane that contains it. We also expect a heteroclinic connection from the periodic orbit to the stable steady state. Crossing from region III to region IV also results in a pitchfork bifurcation, corresponding to a Hopf bifurcation in the center manifold space, but this time of the stable steady state. The resulting periodic orbit is stable and is contained in the x-invariant subspace of the steady state from which it emerges. In general, the two periodic orbits do not have the same amplitude y. A heteroclinic orbit connects them, which corresponds to a trajectory that approaches the frequency of the unstable periodic orbit as $t \to -\infty$ and the frequency of the stable periodic orbit as $t \to \infty$.

Going from region IV back into region I, the two x-invariant subspaces undergo a kind of saddle-node bifurcation in which both the pair of steady states and the pair of periodic orbits annihilate. At this transition, the two periodic orbits therefore have the same amplitude. Finally, we return to the original configuration with no equilibria and a flow-invariant line $y = 0$.

Remark 5.21. The steady-state/Hopf mode interaction (5.19) differs from the Hopf/steady-state mode interaction (5.14). Instead of the simultaneous Hopf bifurcations observed in the Hopf/steady-state case, simultaneous saddle-node and saddle-node of periodic orbits occur.

Case 2: $\varepsilon_p = -1$, $\varepsilon_t = -1$, $\varepsilon_s = 1$. Reversing the sign of ε_s is equivalent to reflecting the phase space across the x-axis and changing stability along the x-direction. The two Hopf transition lines H_+ and H_- exchange location, but the number of equilibria within each region remains unchanged.

Case 3: $\varepsilon_p = -1$, $\varepsilon_t = 1$, $\varepsilon_s = -1$. Reversing the sign of ε_t maps $\mu \to -\mu$ in the bifurcation diagram, that is, reflects the 2-parameter bifurcation diagram of Figure 15 in the λ-axis. In addition, the x-axis is reflected and stability along the y-direction for the equilibria is changed.

Case 4: $\varepsilon_p = -1$, $\varepsilon_t = 1$, $\varepsilon_s = 1$. Reversing the signs of ε_t and ε_s maps $\mu \to -\mu$ as in the previous case. Stability along the y-direction is also changed, but the orientation of the x-axis remains unchanged.

5.4. Hopf/Hopf mode interaction. In the Hopf/Hopf mode interaction, the Jacobian associated with each of the two critical components of the original network has a complex conjugate pair of pure imaginary eigenvalues. We assume that one critical component is downstream from the other, so that the center manifold vector field has the form

$$\begin{aligned} \dot{X} &= f(X), \\ \dot{Y} &= g(X,Y), \end{aligned} \tag{5.20}$$

where $X, Y \in \mathbb{R}^2$. Assume that the origin of (5.20) is a steady state, so that $f(0) = 0$ and $g(0,0) = 0$, and that the Jacobian of (5.15) has two distinct pairs of purely imaginary eigenvalues, namely

$$\operatorname{tr} \mathrm{D}_X f(0) = 0, \qquad \det \mathrm{D}_X f(0) > 0, \qquad \operatorname{tr} \mathrm{D}_Y g(0,0) = 0, \qquad \det \mathrm{D}_Y g(0,0) > 0,$$

with $\det \mathrm{D}_Y g(0,0) \neq \det \mathrm{D}_X f(0)$. Let the eigenvalues associated with the upstream and downstream critical components be $\pm i\omega$ and $\pm i\nu$, respectively. We restrict the following discussion to the nonresonant case in which ω and ν are not rationally related, though the results turn out to also be valid for sufficiently weak resonance. The reason for this restriction is that in the nonresonant case the Birkhoff normal form of the Hopf/Hopf mode interaction commutes with the 2-torus $\mathbb{T}^2$ acting on $\mathbb{R}^4$ by

$$\vec{R}(\theta_x, \theta_y)(X,Y) = (R(\theta_x)X, R(\theta_y)Y), \tag{5.21}$$

where $R(\theta)$ acts on $\mathbb{R}^2$ by counterclockwise rotation through θ.

The goal of this section is more limited in scope than in the previous sections. We begin by assuming that (5.20) is in Birkhoff normal form and use phase-amplitude coordinates to reduce finding steady states and periodic orbits in (5.20) to finding zeros of a map with two one-dimensional nodes that describes the amplitude dynamics of the two-dimensional nodes. We then identify a normal form for the reduced map (5.22) below using equivalences that preserve the feedforward structure of the center manifold network.

Theorem 5.22. *Assume that* (5.20) *has an equilibrium at the origin that undergoes a nonresonant Hopf/Hopf mode interaction. The defining conditions are*

$$\operatorname{tr} \mathrm{D}_X f(0) = 0, \qquad \det \mathrm{D}_X f(0) = \omega^2, \qquad \operatorname{tr} \mathrm{D}_Y g(0,0) = 0, \qquad \det \mathrm{D}_Y g(0,0) = \nu^2,$$

with ω and ν nonzero and irrationally related. Further assume that (5.20) *is in Birkhoff normal form, so $F = (f,g)$ commutes with $\mathbb{T}^2$ under the action* (5.21). *Then there exists a smooth map on $\mathbb{R} \times \mathbb{R}$ of the form*

$$F(x,y) = (r(u)x, s(u,v)y), \tag{5.22}$$

where $u = x^2$, $v = y^2$, $r(0) = 0$, and $s(0,0) = 0$, such that locally solutions to $F(x,y) = 0$ with $y \geq 0$ and $x \geq 0$ are in one-to-one correspondence with solutions to (5.20) *of the four types in Table* 6.

On the reduced system (5.22), the transformations defining equivalence must respect ($\mathbf{Z}_2 \oplus \mathbf{Z}_2$)-symmetry, in addition to the network structure of the center manifold.

Table 6

Four possible types of equilibria in feedforward Hopf/Hopf mode interaction classified by amplitude of the upstream and downstream nodes.

Upstream node	Downstream node	Equilibrium type
$x = 0$	$y = 0$	steady state
$x \neq 0$, $r = 0$	$y = 0$	periodic orbit with period near $2\pi/\omega$
$x = 0$	$y \neq 0$, $s = 0$	periodic orbit with period near $2\pi/\nu$
$x \neq 0$, $r = 0$	$y \neq 0$, $s = 0$	invariant 2-torus

Definition 5.23. *Maps $F(x, y) = (r(u)x, s(u, v)y)$ and $\hat{F}(x, y) = (\hat{r}(u)x, \hat{s}(u, v)y)$ are strongly $(\mathbf{Z}_2 \oplus \mathbf{Z}_2)$-equivalent if there exist $a(u)$, $\phi(u)$, $b(u, v)$, $c(u, v)$, $\psi(u, v)$ such that*

$$\hat{F}(x, y) = \begin{bmatrix} a(u) & 0 \\ b(u, v)xy & c(u, v) \end{bmatrix} \begin{bmatrix} r(\phi^2(u)u)\phi(u)x \\ s(\phi^2(u)u, \psi^2(u, v)v)\psi(u, v)y \end{bmatrix}, \tag{5.23}$$

where $u = x^2$, $v = y^2$ and $a(0)$, $c(0, 0)$, $\phi(0)$, $\psi(0, 0) > 0$.

The normal form is stated in terms of the reduced system (5.22), where the variables x and y represent the amplitudes of periodic motions in the X and Y coordinates of (5.20) on the center manifold, assuming Birkhoff normal form.

Theorem 5.24. *Assume (5.22) satisfies the defining conditions*

$$r(0) = s(0, 0) = 0$$

and the nondegeneracy conditions

$$r_u(0) \neq 0, \quad s_u(0, 0) \neq 0, \quad s_v(0, 0) \neq 0.$$

Then $F(x, y) = (r(u)x, s(u, v)y)$, where $u = x^2$ and $v = y^2$ is strongly $(\mathbf{Z}_2 \oplus \mathbf{Z}_2)$-equivalent to the normal form $\hat{F}(x, y) = (\hat{r}(u)x, \hat{s}(u, v)y)$ given by

$$\begin{aligned} \hat{r}(u)x &= \varepsilon_p u x, \\ \hat{s}(u, v)y &= (\varepsilon_q u + \varepsilon_t v)\, y, \end{aligned} \tag{5.24}$$

where

$$\varepsilon_p = \operatorname{sign}(r_u(0)), \quad \varepsilon_q = \operatorname{sign}(s_u(0, 0)), \quad \varepsilon_t = \operatorname{sign}(s_v(0, 0)).$$

We note that remarks on genericity that are similar to those made after Theorem 5.11 also hold for this codimension-2 bifurcation.

To classify all possible perturbations of the normal form (5.24) up to equivalence, we compute a universal unfolding.

Theorem 5.25. *The normal form (5.24) has codimension-2. A universal unfolding is*

$$\begin{aligned} r(u)x &= (\lambda + \varepsilon_p u)\, x, \\ s(u, v)y &= (\mu + \varepsilon_q u + \varepsilon_t v)\, y. \end{aligned} \tag{5.25}$$

Table 7

Hopf/Hopf mode interaction. Case 1: List of equilibria (column 3) and their stabilities (column 4) in each of the regions (column 1) in Figure 16 (left).

	Region	Equilibria (x, y)	Eigenvalues
I	$\lambda < 0$ $\mu < 0$	$(0,0)$	$--$
II	$\lambda < 0$ $0 < \mu$	$(0,0)$ $\left(0, \sqrt{\mu}\right)$	$-+$ $--$
III	$0 < \lambda$ $\lambda < \mu$	$(0,0)$ $\left(0, \sqrt{\mu}\right)$ $\left(\sqrt{\lambda}, 0\right)$ $\left(\sqrt{\lambda}, \sqrt{\mu - \lambda}\right)$	$++$ $+-$ $-+$ $--$
IV	$0 < \mu$ $\mu < \lambda$	$(0,0)$ $\left(0, \sqrt{\mu}\right)$ $\left(\sqrt{\lambda}, 0\right)$	$++$ $+-$ $--$
V	$\mu < 0$ $0 < \lambda$	$(0,0)$ $\left(\sqrt{\lambda}, 0\right)$	$+-$ $--$

It is now straightforward to compute the steady-state solutions of (5.25) as a function of the parameters μ and λ. Solutions with one of x or y equal to zero correspond to periodic solutions of (5.20), and those where both x and y are nonzero correspond to invariant tori. Changing $\varepsilon_p, \varepsilon_q, \varepsilon_t$ to $-\varepsilon_p, -\varepsilon_q, -\varepsilon_t$ rotates the transition variety in the $\mu\lambda$-plane by 180° and changes the stability of all solutions in both the x- and the y-directions. Hence we assume $\varepsilon_p = -1$ and consider the resulting four cases.

Case 1: $\varepsilon_p = \varepsilon_q = \varepsilon_t = -1$. The Jacobian at an equilibrium (x, y) is

$$J = \begin{bmatrix} \lambda - 3x^2 & 0 \\ -2xy & \mu - 3x^2 - 3y^2 \end{bmatrix}.$$

There is an equilibrium $x = y = 0$ for all values of μ and λ, with eigenvalues λ and μ. The lines $\mu = 0$ and $\lambda = 0$ correspond to Hopf bifurcations in the full system, creating periodic solutions with $y = \sqrt{\mu}$ and $x = \sqrt{\lambda}$, respectively. When $\lambda > 0$, there is an invariant cylinder $x = \sqrt{\lambda}$. There are also two torus bifurcations. One occurs on the half-line $\lambda = 0$, $\mu \geq 0$ and the other on the half-line $\lambda = \mu$, $\mu \geq 0$. The steady states and their stabilities are listed in Table 7 and shown in Figure 16.

Case 2: $\varepsilon_p = \varepsilon_q = -1$, $\varepsilon_t = 1$. Changing the sign of ε_t (from Case 1) changes the criticality of the bifurcations which create the equilibria at $(x, y) = \left(0, \sqrt{\frac{-\mu}{\varepsilon_t}}\right)$ and $\left(\sqrt{\lambda}, \sqrt{\frac{-(\varepsilon_q \lambda + \mu)}{\varepsilon_t}}\right)$. Bifurcation curves, however, remain unchanged. See Figure 16.

Case 3: $\varepsilon_p = -1$, $\varepsilon_t = \varepsilon_q = 1$. Changing the sign of ε_q and ε_t (from Case 1) is equivalent to changing the sign of μ together with a change of stability in the y-direction.

Case 4: $\varepsilon_p = \varepsilon_t = -1$, $\varepsilon_q = 1$. Changing the sign of ε_q and ε_t (from Case 2) is equivalent to changing the sign of μ together with a change of stability in the y-direction.

Appendix A. Reduction procedure for networks with higher-dimensional nodes.

We describe a construction that converts any fully inhomogeneous network $\mathcal{G}$ with higher-

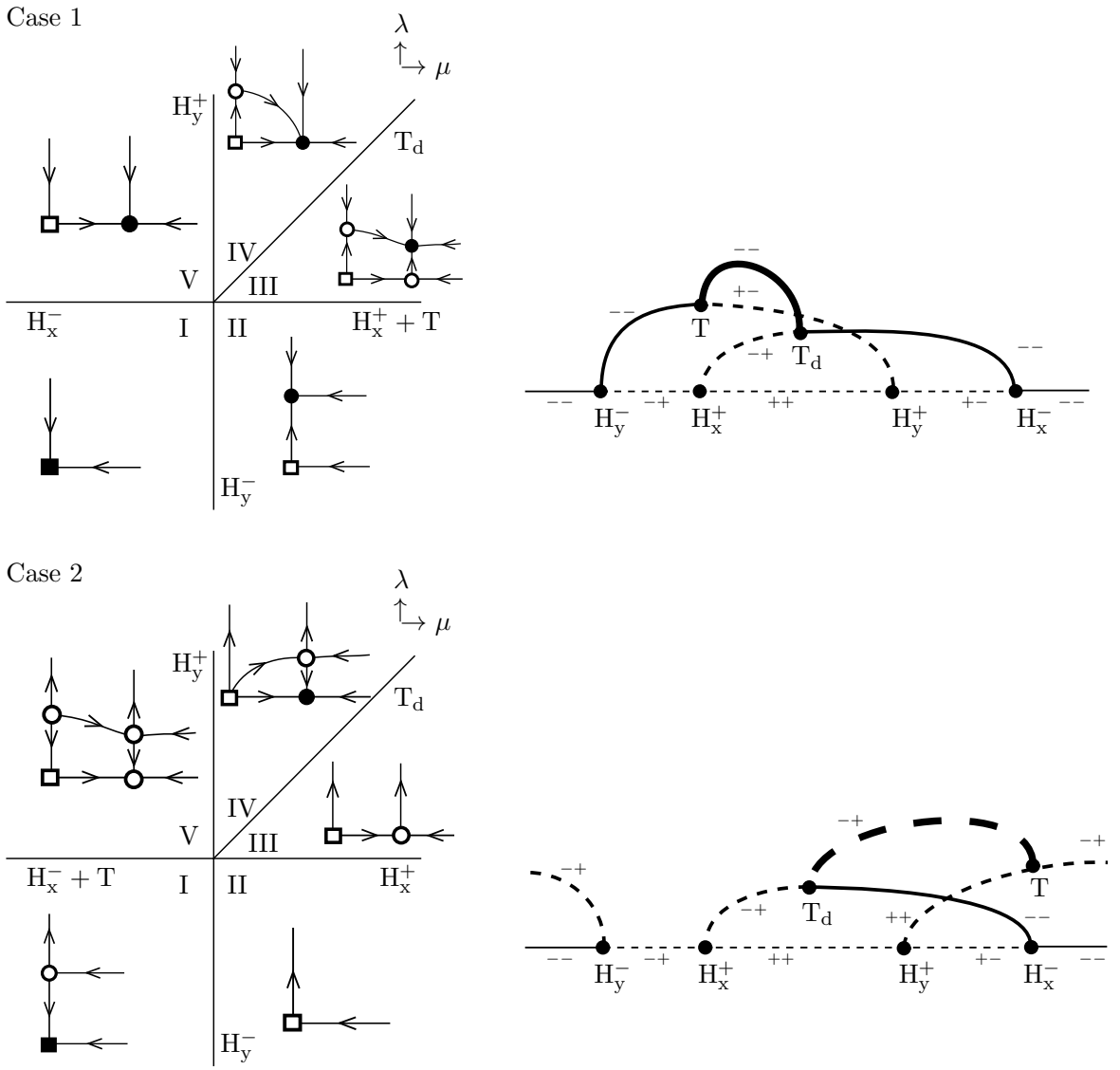

Figure 16. *Hopf/Hopf mode interaction: Cases* 1 *and* 2. Left*: bifurcation sets (bold lines) in the* $\mu\lambda$*-plane, with phase portraits in the* xy*-plane for each region of parameter space.* Right*: bifurcation diagram as a small circle is traversed around the origin in the* $\mu\lambda$*-plane, starting in the third quadrant. Dots indicate bifurcations, and small plus and minus signs show the stability of each branch in the* x*- and the* y*-directions. Lines of medium thickness (solid or dashed) indicate periodic solutions in the full four-dimensional system. Very thick lines linking these branches represent the invariant torus. In Case* 1*, solid lines* H_y^-*,* H_y^+*,* H_x^-*, and* T_d *represent pitchfork bifurcations for* (5.25)*, and* $H_x^+ + T$ *represents a double pitchfork bifurcation for* (5.25)*. They correspond to Hopf, Hopf, Hopf, torus, and Hopf plus torus bifurcations, respectively, for* (5.20)*. In Case* 2*, labels are the same, except the torus bifurcation* T *occurs with* H_x^- *rather than* H_x^+*.*

dimensional node phase spaces P_c into a fully inhomogeneous network $\mathcal{G}^\dagger$ with one-dimensional node phase spaces, without changing the space of admissible maps, when variables are suitably

identified. We call $\mathcal{G}^\dagger$ the *expansion* of $\mathcal{G}$.

Let $\mathcal{G}$ be fully inhomogeneous with nodes $\mathcal{C} = \{1, \dots, n\}$ and arrows $\mathcal{E}$. In the single-arrow formalism of Stewart, Golubitsky, and Pivato (2003), which applies to the fully inhomogeneous case, each arrow $e \in \mathcal{E}$ can be identified with the pair

$$(\text{head}(e), \text{tail}(e)) \in \mathcal{C} \times \mathcal{C},$$

and distinct arrows give distinct pairs. Also, the input set $I(c)$ consists of arrows whose head is c. In this case, the set $I(c)$ can be identified with the set of tail nodes $\{\text{tail}(e) : e \in I(c)\}$. Note that $c \notin I(c)$, so the pair (c, c) does not appear as an arrow.

Assume that $\dim P_c = \delta(c) \geq 1$ for $c \in \mathcal{C}$.

Definition A.1. *Given $\mathcal{G}$, fully inhomogeneous, we define the* expansion $\mathcal{G}^\dagger$ *as follows. Nodes and arrows are defined by*

$$\begin{aligned} \mathcal{C}^\dagger &= \{[c,k] : 1 \leq k \leq \delta(c)\}, \\ \mathcal{E}^\dagger &= \{([c,k],[d,l]) : (c,d) \in \mathcal{E}, 1 \leq k \leq \delta(c), 1 \leq l \leq \delta(d)\} \\ &\qquad \cup \{([c,k],[c,m]) : 1 \leq k, m \leq \delta(c), k \neq m\}, \end{aligned}$$

where for clarity, ordered pairs are denoted by square brackets $[c,k]$. Each node c is expanded to a clump of nodes $[c,k]$, where $1 \leq k \leq \delta(c)$. Each input arrow $e = (c,d)$ of c is expanded to a bundle of arrows between nodes in the corresponding clumps, one for each pair of heads and tails $[c,k]$ and $[d,l]$. Moreover, there are arrows between all distinct $[c,k],[c,m]$; that is, each clump is "internally" all-to-all connected.

Heads and tails in $\mathcal{G}^\dagger$ are defined by the pairs of nodes. All node types and arrow types are distinct.

The simplest way to describe this construction is in terms of the *adjacency matrix* $A = A(\mathcal{G})$, defined by

$$A_{ij} = 1 \iff (i,j) \in \mathcal{E} \text{ or } i = j.$$

Then $A^\dagger = A(\mathcal{G}^\dagger)$ is obtained from A by replacing every entry A_{ij} by a block matrix B^{ij} of size $\delta(i) \times \delta(j)$, whose entries are all the same as A_{ij}, that is, all 0's or all 1's.

Observe that $\mathcal{G}^\dagger$ is fully inhomogeneous since by definition all node types and arrow types are distinct.

Example A.2. The 3-node network $\mathcal{G}$ of Figure 17 (left) gives the expansion $\mathcal{G}^\dagger$ of Figure 17 (right) when $\dim P_1 = 3, \dim P_2 = \dim P_3 = 2$.

The adjacency matrix for $\mathcal{G}$ is

$$A(\mathcal{G}) = \begin{bmatrix} 1 & 1 & 0 \\ 0 & 1 & 1 \\ 1 & 1 & 1 \end{bmatrix}$$

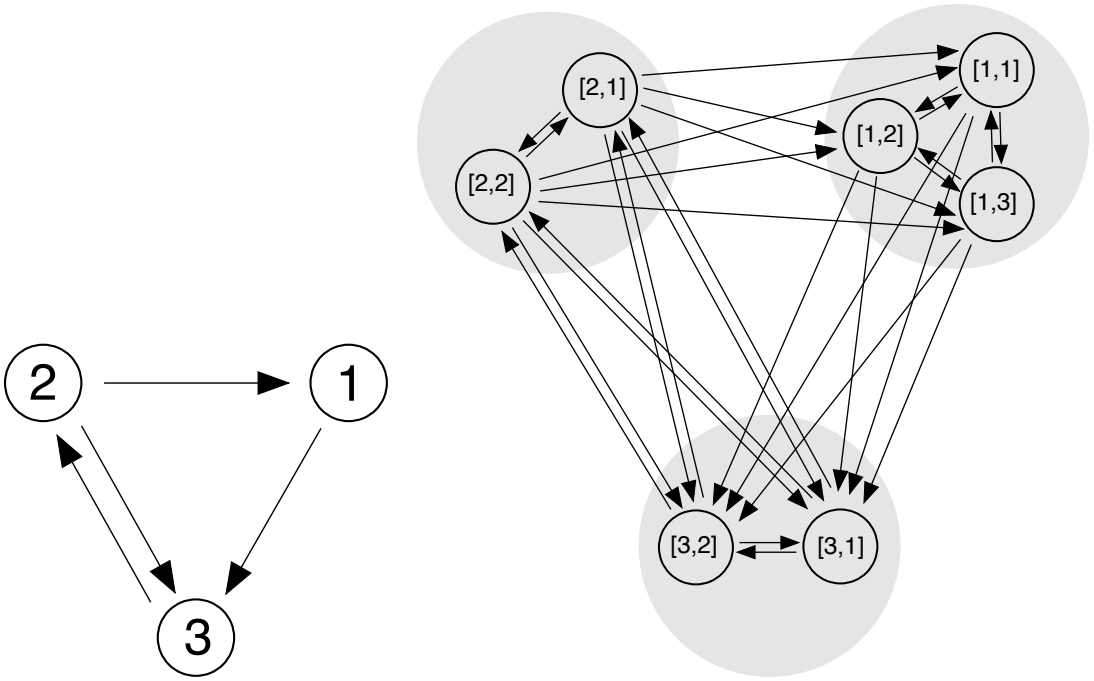

Figure 17. Left*: A fully inhomogeneous network* $\mathcal{G}$. Right*: The expansion* $\mathcal{G}^\dagger$ *when* $\dim P_1 = 3, \dim P_2 = \dim P_3 = 2$. *(All arrows and nodes have distinct types.)*

and that of $\mathcal{G}^\dagger$ is

$$A(\mathcal{G}^\dagger) = \left[\begin{array}{ccc|cc|cc} 1 & 1 & 1 & 1 & 1 & 0 & 0 \\ 1 & 1 & 1 & 1 & 1 & 0 & 0 \\ 1 & 1 & 1 & 1 & 1 & 0 & 0 \\ \hline 0 & 0 & 0 & 1 & 1 & 1 & 1 \\ 0 & 0 & 0 & 1 & 1 & 1 & 1 \\ \hline 1 & 1 & 1 & 1 & 1 & 1 & 1 \\ 1 & 1 & 1 & 1 & 1 & 1 & 1 \end{array}\right].$$

For both networks, the diagonal entries 1 come from the nodes, whereas the off-diagonal entries 1 in any diagonal block of $A(\mathcal{G}^\dagger)$ come from the all-to-all connections within that clump.

Clearly, for any i the input set $I([c,i])$ in $\mathcal{G}^\dagger$ is

$$I([c,i]) = (I(c))^\dagger = \{[d,j] : d \in I(c)\}.$$

Next, we define how to interpret an admissible map f for $\mathcal{G}$ as an admissible map $f^\dagger$ for $\mathcal{G}^\dagger$. For each node $[c,i]$ of $\mathcal{G}^\dagger$, let

$$P_{[c,i]} = \mathbb{R}.$$

Then we identify

$$\mathbb{R}^{\delta(c)} = P_c = \bigoplus_i P_{[c,i]}$$

so that the $x_{[c,i]}$ are coordinates on P_c.

Now a map $f : P \to P$ with components $f_c : P_c \to P$ can be split into finer components

$$f_{[c,i]}(x) = (f(x))_{[c,i]},$$

where $x \in P$ can be identified with its component representations $(x_c)_{c\in\mathcal{C}} \in \oplus P_c$ and $(x_{[c,i]})_{[c,i]\in\mathcal{C}^\dagger} \in \oplus P_{[c,i]}$. We then have the following.

Theorem A.3. *Let $\mathcal{G}$ be fully inhomogeneous. A map f is $\mathcal{G}$-admissible if and only if, when represented in the natural manner using coordinates indexed by the $[c,k]$, it is $\mathcal{G}^\dagger$-admissible.*

Proof. In a fully inhomogeneous network, the only constraint on an admissible map is the domain condition. The adjacency matrices show that this holds for $f^\dagger$ if and only if it holds for f. That is, f_c depends only on the x_j for $j \in I(c)$ if and only if all $f_{[c,i]}$ depend only on the $x_{[j,k]}$ for $[j,k] \in I([c,i]) = (I(c))^\dagger$. All components are otherwise arbitrary.

Remark A.4. (a) Expansion preserves path components in the sense that the union of the clumps of a path component in $\mathcal{G}$ is the corresponding path component in $\mathcal{G}^\dagger$.

(b) Expansion also preserves "upstream/downstream," that is, the natural feedforward ordering between path components.

REFERENCES

S. Allesina and M. Pascual (2008), *Network structure, predator-prey modules, and stability in large food webs*, Theor. Ecol., 1, pp. 55–64.

J. Best, H. F. Nijhout, and M. Reed (2010), *Serotonin synthesis, release and reuptake in terminals: A mathematical model*, Theor. Biol. Med. Model, 7, 34.

P. Boldi and S. Vigna (2002), *Fibrations of graphs*, Discrete Math., 243, pp. 21–66.

M. T. Borisuk and J. J. Tyson (1998), *Bifurcation analysis of a model of mitotic control in frog eggs*, J. Theor. Biol., 195, pp. 69–85.

J. Carr (1981), *Applications of Centre Manifold Theory*, Springer, New York.

C. Chen, D Zhang, T. R. Hazbuz, and M. Zhang (2019), *Inferring gene regulatory networks from a population of yeast segregants*, Sci. Rep., 9, 1197, https://doi.org/10.1038/s41598-018-37667-4.

L. Deville and E. Lerman (2015), *Modular dynamical systems on networks*, J. Eur. Math. Soc. (JEMS), 17, pp. 2977–3013.

T. Elmhirst and M. Golubitsky (2006), *Nilpotent Hopf bifurcations in coupled cell systems*, SIAM J. Appl. Dyn. Syst., 5, pp. 205–251, https://doi.org/10.1137/050635559.

D. Eppstein (2016), *Design and Analysis of Algorithms*, CS/CSE 161, U. California, Irvine, https://www.ics.uci.edu/~eppstein/161/960220.html.

G. F. Fussmann and G. Heber (2002), *Food web complexity and chaotic population dynamics*, Ecol. Lett., 5, pp. 394–401.

M. Golubitsky and C. Postlethwaite (2012), *Feed-forward networks, center manifolds, and forcing*, Discrete Contin. Dyn. Syst., 32, pp. 2913–2935.

M. Golubitsky, D. Romano, and Y. Wang (2010), *Network periodic solutions: Full oscillation and rigid synchrony*, Nonlinearity, 23, pp. 3227–3243.

M. Golubitsky, D. Romano, and Y. Wang (2012), *Network periodic solutions: Patterns of phase-shift synchrony*, Nonlinearity, 25, pp. 1045–1074.

M. Golubitsky and D. G. Schaeffer (1985), *Singularities and Groups in Bifurcation Theory: Vol.* I, Appl. Math. Sci. 51, Springer, New York.

M. Golubitsky and I. Stewart (2006), *Nonlinear dynamics of networks: The groupoid formalism*, Bull. Amer. Math. Soc. (N.S.), 43, pp. 305–364.

M. Golubitsky and I. Stewart (2017), *Coordinate changes that preserve admissible maps for network dynamics*, Dyn. Syst., 32, pp. 81–116.
M. Golubitsky, I. Stewart, and A. Török (2005), *Patterns of synchrony in coupled cell networks with multiple arrows*, SIAM J. Appl. Dyn. Syst., 4, pp. 78–100, https://doi.org/10.1137/040612634.
M. Golubitsky and Y. Wang, *Infinitesimal homeostasis in three-node input-ouput networks*, submitted.
J. Guckenheimer and P. Holmes (1983), *Nonlinear Oscillations, Dynamical Systems, and Bifurcations of Vector Fields*, Springer, New York.
F. Harary (1994), *Digraphs*, in Graph Theory, Addison–Wesley, Reading, MA.
R. Joly (2012), *Observation and inverse problem in coupled cell networks*, Nonlinearity, 25, pp. 657–676.
M. C. A. Leite and M. Golubitsky (2006), *Homogeneous three-cell networks*, Nonlinearity, 19, pp. 2313–2363.
J. Lu, X. Yu, G. Chen, and W. Yu, eds. (2016), *Complex Systems and Networks*, Springer, Berlin.
J. Martinet (1982), *Singularities of Smooth Functions and Maps*, Cambridge University Press, Cambridge, UK.
R. Milo, S. Shen-Orr, S. Itzkovitz, N. Kashtan, D. Chklovskii, and U. Alon (2002), *Network motifs: Simple building blocks of complex networks*, Science, 298, pp. 824–827.
M. Newman, L. Barabási, and D. J. Watts (2006), *The Structure and Dynamics of Networks*, Princeton Stud. Complex., Princeton University Press, Princeton, NJ.
E. Nijholt (2018), *Bifurcations in Network Dynamical Systems*, Ph.D. thesis, Vrije Universiteit, Amsterdam.
E. Nijholt, B. Rink, and J. Sanders (2016), *Graph fibrations and symmetries of network dynamics*, J. Differential Equations, 261, pp. 4861–4896.
E. Nijholt, B. Rink, and J. Sanders (2017), *Center manifolds of coupled cell networks*, SIAM J. Math. Anal., 49, pp. 4117–4148, https://doi.org/10.1137/16M106861X.
B. Rink and J. Sanders (2014), *Coupled cell networks and their hidden symmetries*, SIAM J. Math. Anal., 46, pp. 1577–1609, https://doi.org/10.1137/130916242.
B. Rink and J. Sanders (2015), *Coupled cell networks: Semigroups, Lie algebras, and normal forms*, Trans. Amer. Math. Soc., 367, pp. 3509–3548, https://doi.org/10.1090/S0002-9947-2014-06221-1.
B. S. W. Schröder (2002), *Ordered Sets: An Introduction*, Birkhäuser, Boston.
P. Soares (2018), *The lifting bifurcation problem on feed-forward networks*, Nonlinearity, 31, 5500, https://doi.org/10.1088/1361-6544/aae1d0.
I. Stewart (2004), *Networking opportunity*, Nature, 427, pp. 601–604.
I. Stewart (2014), *Synchrony-breaking bifurcations at a simple real eigenvalue for regular networks 2: Higher-dimensional cells*, SIAM J. Appl. Dyn. Syst., 13, pp. 129–156, https://doi.org/10.1137/130917636.
I. Stewart and M. Golubitsky (2011), *Synchrony-breaking bifurcation at a simple real eigenvalue for regular networks 1: 1-dimensional cells*, SIAM J. Appl. Dyn. Syst., 10, pp. 1404–1442, https://doi.org/10.1137/110825418.
I. Stewart, M. Golubitsky, and M. Pivato (2003), *Symmetry groupoids and patterns of synchrony in coupled cell networks*, SIAM J. Appl. Dyn. Syst., 2, pp. 609–646, https://doi.org/10.1137/S1111111103419896.
J. Tyson and B. Novak (2010), *Functional motifs in biochemical reaction networks*, Annu. Rev. Phys. Chem., 61, pp. 219–240.